Path Following of a Quadrotor with a Cable-Suspended Payload

Technical Report 001/2021

Adeel Akhtar Sajid Saleem Jinjun Shan [12]

September 12, 2021

Contents

Abstract

Aerial robots and drone-based payload delivery is in the spotlight and is considered revolutionary for the logistics and transportation sectors. In most use cases, the payload is required to precisely follow a given path for safe and secure operation in a cluttered environment. This work addresses the problem of designing a path following controller for a point-mass payload tethered to a quadrotor. Specifically, we design a smooth dynamic feedback controller that forces the suspended load to converge and follow a large class of both closed and non-closed embedded curves. Using a local representation of the dynamical system consisting of a quadrotor and the cable-suspended payload, we show that the system has a well-defined vector relative degree. We treat the given curve as a smooth manifold and then use set stabilization to find the maximal control invariant manifold. The resulting controller guarantees that once the system reaches the path, it stays on the path indefinitely. We demonstrate the performance of the proposed controller through extensive simulations with practical sensor noise and parametric uncertainties. Moreover, successful real-world experimental validation of the proposed controller is demonstrated on a Quanser QDrone UAV platform with a cable-suspended payload.

1 Introduction

Mobile robots, in particular unmanned aerial vehicles (UAVs), have gained central importance because of their vast applications in areas as diverse as surveillance, agriculture, warehouse inventory management, last-mile delivery, fire extinguishing, and disaster relief operations. Specifically, multi-rotors UAVs such as quadrotors have achieved immense popularity among industrial and academic research communities because of its simple mechanical design, low-cost structure, vertical take-off and landing (VTOL) ability, and agile dynamics [1, 2]. In recent years, there has been an increased demand for efficient aerial transportation of light to medium payload (up to few kilograms), and a quadrotor can be an excellent choice for such a mission due to its compact size and relatively higher thrust generation capability [3, 4].

Broadly speaking, there are two approaches to attach a payload with a quadrotor, i.e., active and passive attachment [5]. The former approach requires a gripper attached to the body of the quadrotor. Although the gripper mechanism provides an additional degree of freedom and the capability of aerial manipulation, it comes at the cost of loss of agility due to an undesirable increase in inertia. The passive attachment uses a cable attached to the quadrotor at one end and the load to the other end. The cable suspension approach provides an agile platform and better manoeuvrability [6]; however, it brings its own challenges in the controller design because of an additional degree of under-actuation. In this work, we deal with the latter approach, i.e., a quadrotor system attached with a cable suspended point-mass, as shown in Figure 1.1.

In this paper, we consider a path following problem for the system consisting of a quadrotor attached with a cable suspended load. Given a non-self-intersecting smooth curve in three-dimensional space and a quadrotor system attached with a cable suspended load, our objective is to design a smooth dynamic controller such that the cable-suspended load converges to the given path and follows it. Unlike a trajectory, a path is a set of points without a timing law associated with it. A path following problem and a trajectory tracking problem are related to each other, but former is more general since a path can be treated as a set of trajectories [7, 8]. For example, there exist such instances where a path following can be solved but the corresponding trajectory tracking problem has no solution [9, 10]. A key advantage of the path following framework is that it allows the system to achieve path invariance, i.e., once the system

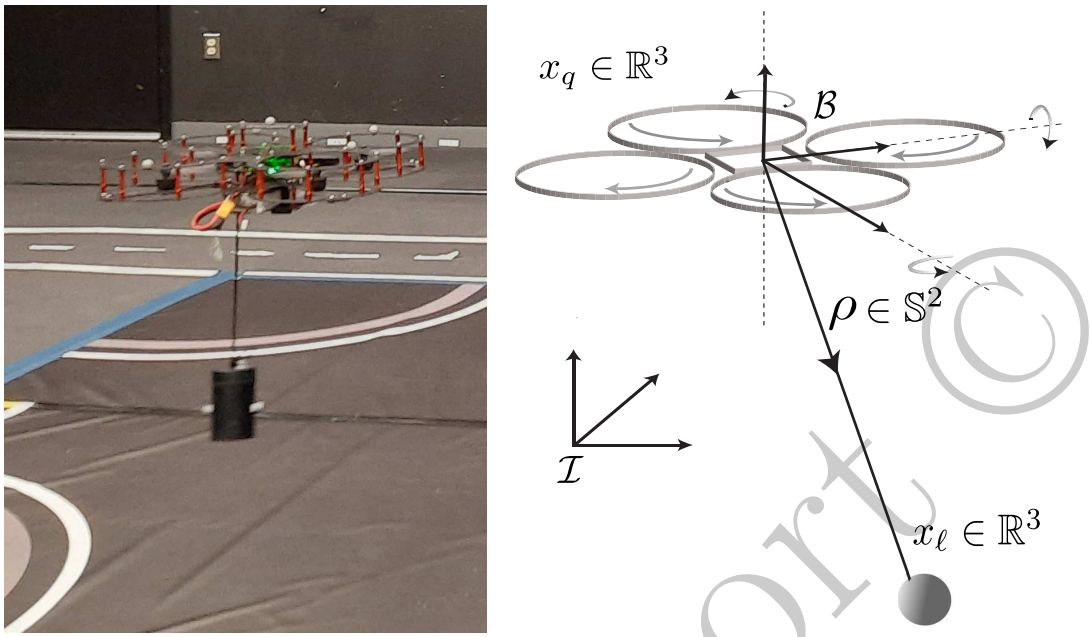

Figure 1.1: Quadrotor with a cable-suspended payload. On the left is Quanser QDrone UAV attached with a cable-suspended payload during flight. On the right is the schematic diagram of a typical quadrotor with a cable suspended point mass.

converges to the given path, it stays on the path indefinitely [7]. Moreover, path following approach precludes the planning and design of optimal trajectory characterized by the minimum jerk or minimum snap, which is a requirement for most of the trajectory tracking problems for the system under consideration [11]. Although path following approach has been applied to the quadrotor system [12,13], there is no prior work that deals with path following of the load suspended to a quadrotor through a cable for the class of regular embedded curves.

It is well known that the configuration space of a quadrotor or a quadrotor attached with a cable suspended load is a smooth manifold [14]. In literature, approaches to the design of a controller for non-linear systems evolving on a manifold can be classified into coordinate free (or geometric) and local coordinate-based methods [15]. The geometric methods employ a hierarchical controller design framework based upon an inner-outer loop approach, which provides singularity-free control laws [16–19]. The inner loop stabilizes the attitude of the system, whose convergence is followed by the convergence of the outer loop, which stabilizes the position of the load. Although this cascade control design method leads to a simpler design approach, however, the stability of the individual loops does not automatically guarantee the convergence of the overall system, for which the stability must be justified independently. One of the shortcomings of almost every existing geometric control method for the given system is that these methods are intended to track a time-parameterized trajectory [5, 17, 19, 20]. , which

has performance limitations as highlighted in [9]. Moreover, such trajectory tracking controllers cannot guarantee precise path following in the sense that once they converge to the trajectory, the system may leave the trajectory [21, 22].

The second approach, i.e., the coordinate-based method using local charts leads to local controllers that suffer singularities, such as gimbal lock [23, 24]. This local representation imposes a slight restriction on the flight envelope of the system, as the roll and pitch angles of the quadrotor must remain within $\left(-\frac{\pi}{2}, \frac{\pi}{2}\right)$. Despite this constraint, a large class of both closed and non-closed curves can be followed without approaching singularity [25].

In this paper, we consider a local coordinate-based approach, i.e., Euler angle representation; therefore, to no surprise, our results are local [25]. However, unlike existing approaches applied to the design of controllers for the system with a quadrotor and a suspended load, we do not follow a cascade (inner-outer loop) structure and instead propose a monolithic approach. To the best of our knowledge, this is the first time that the monolithic design approach is being proposed for the system under study. This design approach neither requires an assumption of time separation between quadrotor attitude dynamics and quadrotor position dynamics, nor a time-scale separation between the quadrotor and the load [12]. Moreover, another distinction between our work and the prior research work is that we propose a novel smooth dynamic feedback controller that guarantees path invariance. In other words, once the controller brings the payload to the path, the payload stays on the path indefinitely, while maintaining the desired position, velocity or acceleration profile. Given an *a priori* non-self intersecting path, the proposed path following controller enables operation of quadrotor carrying a cable suspended load in challenging environments that require aggressive maneuvers, such as congested or low clearance indoor space, corridors, and slalom courses.

Significantly less attention has been given to the path following problem compared to the trajectory tracking problem. In [26], the authors also consider a similar problem to the one we consider in this paper, i.e., a path following problem for a quadrotor system attached with a payload via suspended cable. The key difference between our work and [26] is that the latter presents an inner-outer loop control approach based on reduction theorems, which allows the system to follow only straight lines. In [26], if the desired path is not straight, then it needs to be approximated by a series of straight lines, and the controller must switch from one segment to the other. Our proposed approach neither requires a piece-wise approximation of the desired path nor switching while following challenging curves.

1.1 Contributions

We have made the following contributions.

1. We have proposed a novel dynamic transverse feedback linearizing controller that allows the cable suspended load attached to the quadrotor to follow a large class

of both closed and non-closed curves.

2. Using a local coordinate approach, we have established that the system has a well-defined vector relative degree in the neighborhood of a large class of curves (Theorem 4.0.5), and have proved that after dynamic extension, the system is diffeomorphic to a chain of integrators (Corollary 4.0.6).

3. Our proposed technique differs from all existing methods that deal with quadrotor and cable suspended load in the sense that our novel controller guarantees path invariance for a class of curves.

4. Validation of the proposed controller design on a hardware platform consisting of a Quanser QDrone and a cable suspended load.

The rest of the paper is organized as follows. After presenting math preliminaries, we introduce the dynamic model of the quadrotor attached with cable suspended load in Section 2. The formal statement of the path following problem for the system under consideration is presented in Section 3. In Section 4, we present details of the controller design, provide closed-form expression of the dynamic controller, and prove the main result. Numerical simulation results under practical scenarios are discussed in Section 4.2, and the numerical performance results for experimental validation are presented in 5 . Finally, conclusions are drawn in Section 6.

1.2 Notation and math preliminaries

The symbol $:=$ denotes equal by definition. The set of natural number is denoted by $\mathbb{N}$. The standard n-dimensional Euclidean space is an $\mathbb{R}$-vector space denoted by $\mathbb{R}^n$ and it consists of ordered n-tuples $(x_1, \ldots, x_n)$, where each $x_i \in \mathbb{R}$, for $i \in \{1, 2, \ldots, n\}$. Sometimes it is convenient to represent elements of the Euclidean vector space as $n \times 1$ matrices, i.e., column vectors, and is denoted by $x = \text{col}(x_1, \ldots, x_n)$, for $x \in \mathbb{R}^n$. An i-dimensional column vector consisting of all zeros is denoted by 0_i. Given $A \in \mathbb{R}^{m \times n}$, its transpose is given by $A^\top \in \mathbb{R}^{n \times m}$. The standard inner product on $\mathbb{R}^n$ is denoted by $\langle \cdot, \cdot \rangle : \mathbb{R}^n \times \mathbb{R}^n \to \mathbb{R}$, and the standard norm is denoted by $\|\cdot\| : \mathbb{R}^n \to \mathbb{R}$. A point to set distance, for a point $x \in \mathbb{R}$ and a set $S \subset \mathbb{R}^n$, is represented by $\|x\|_S := \inf_{y \in S} \|x - y\|$. The cross product of two vectors in the three dimensional Euclidean space is given by $\times$. Let C_i, S_i, and T_i denote $\cos(i)$, $\sin(i)$, and $\tan(i)$, respectively, for $i \in \{\phi, \theta, \psi\}$. The composition of two maps, $h : A \to B$ and $s : B \to C$, is represented by $s \circ h : A \to C$. A parameterized curve σ in $\mathbb{R}^n$ is a map $\sigma : \mathbb{D} \to \mathbb{R}^n$, where the domain $\mathbb{D} = \mathbb{R}$ for non-closed curves, and $\mathbb{D} = \mathbb{R} \bmod P$ for closed curves of period P. For a P-periodic closed parameterized curve σ, $\sigma(\lambda + P) = \sigma(\lambda)$. Let $f : \mathbb{R}^n \to \mathbb{R}^m$ be a C^1 map and $p \in \mathbb{R}^n$, the derivative of f at p is denoted by $df_p := \frac{\partial f}{\partial x}\Big|_{x=p}$. For C^∞ maps $f, g : \mathbb{R}^n \to \mathbb{R}^n$ and a C^∞ map $\lambda : \mathbb{R}^n \to \mathbb{R}$, the iterative Lie derivatives are defined as $L_g^0 \lambda := \lambda$, $L_g^k \lambda := L_g(L_g^{k-1}\lambda)$, $L_g L_f \lambda := L_g(L_f \lambda)$.

2 Dynamic model

In this article, we consider a quadrotor and a payload, which is attached to the center of gravity of the quadrotor by a cable. We made the following assumption.

Assumption 1. *The cable has zero mass and it cannot be stretched. The mass of the payload, which is assumed to be a point-mass, is less than the maximum payload of the quadrotor. Furthermore, the tension in the cable is assumed to be positive for all time* [1].

Let $\mathcal{I} := \{e_1, e_2, e_3\}$ be the fixed inertial frame and $\mathcal{B} := \{b_1, b_2, b_3\}$ be the body frame attached to the center of mass of the quadrotor. Let $x_q(t) \in \mathbb{R}^3$ and $v_q(t) \in \mathbb{R}^3$ be the position and velocity of the quadrotor, respectively, and $x_\ell(t) \in \mathbb{R}^3$ and $v_\ell(t) \in \mathbb{R}^3$ be the position and velocity of the load, respectively. Let $m_\ell \in \mathbb{R}$ and $m_q \in \mathbb{R}$ be the mass of the payload and mass of the quadrotor, respectively, and $g \in \mathbb{R}$ be the acceleration due to gravity. Let $b_3 = \text{col}(0, 0, 1)$ be the unit vector in z direction. Let $u_t(t) \in \mathbb{R}$ be the total thrust produced by all four propellers of the quadrotor along the z-axis of the body axis, and is assumed to be non-zero. Let $\rho(t) \in \mathbb{S}^2$ be the unit vector from the quadrotor to the load. Let $L \in \mathbb{R}$ and $T > 0 \in \mathbb{R}$ be the length of the cable and its tension, respectively. The position of the quadrotor and the position of the load are related by

$$x_q(t) = x_\ell(t) - L\rho(t). \tag{2.1}$$

Let $\Omega(t) := \text{col}(\Omega_1(t), \Omega_2(t), \Omega_3(t)) \in \mathbb{R}^3$ be the body rates of the quadrotor, $J := \text{diag}(J_x, J_y, J_z) \in \mathbb{R}^{3\times3}$ be the inertia of the quadrotor with respect to the three axes of $\mathcal{B}$. Similarly, we define the total moments about the body axes by $\tau(t) := \text{col}(\tau_1(t), \tau_2(t), \tau_3(t)) \in \mathbb{R}^3$, which along with the thrust $u_t(t)$ constitute the four inputs of the system under consideration. We assume that the orientation $R(t) \in \mathsf{SO}(3)$ of the quadrotor is represented locally by three Euler angles, i.e., roll-pitch-yaw $\Phi(t) := \text{col}(\phi(t), \theta(t), \psi(t)) \in \mathbb{R}^3$. The dynamics of the quadrotor with a cable suspended

[1] For a model that allows non-negative tension in the cable, hybrid control techniques can be used to design a controller, for details see [27].

Table 2.1: Parameters and states of the system

Description	Symbols
fixed inertial frame	$\mathcal{I} := \{e_1, e_2, e_3\}$
quadrotor's body frame	$\mathcal{B} := \{b_1, b_2, b_3\}$
constant cable length	$L \in \mathbb{R}$
cable tension	$T \in \mathbb{R}$
unit vector from quadrotor to the payload	$\rho \in \mathbb{S}^2$
constant mass of the quadrotor	$m_q \in \mathbb{R}$
constant mass of the payload	$m_\ell \in \mathbb{R}$
position of the the quadrotor	$x_q \in \mathbb{R}^3$
position of the payload	$x_\ell \in \mathbb{R}^3$
velocity of the quadrotor	$v_q \in \mathbb{R}^3$
velocity of the the payload	$v_\ell \in \mathbb{R}^3$
thrust control input	$u_t \in \mathbb{R}$
torque input of the quadrotor	$\tau := \text{col}(\tau_1, \tau_2, \tau_3) \in \mathbb{R}^3$
constant inertia of the quadrotor	$J := \text{diag}(J_x, J_y, J_z) \in \mathbb{R}^{3\times 3}$
constant acceleration due to gravity	$g \in \mathbb{R}$
quadrotor body rates	$\Omega := \text{col}(\Omega_1, \Omega_2, \Omega_3) \in \mathbb{R}^3$
rotation matrix of quadrotor from $\mathcal{B}$ to $\mathcal{I}$	$R \in \mathsf{SO}(3)$
Euler angles (roll, pitch, yaw)	$\Phi := \text{col}(\phi, \theta, \psi)$

load [27, 28], can be locally represented[2] as

$$\begin{aligned} \dot{x}_\ell &= v_\ell \\ m_\ell \dot{v}_\ell &= -T\rho - m_\ell g b_3 \\ \dot{x}_q &= v_q \\ m_q \dot{v}_q &= u_t R b_3 - m_q g b_3 + T\rho \\ \dot{\Phi} &= M\Omega \\ J\dot{\Omega} &= \tau - (\Omega \times J\Omega), \end{aligned} \tag{2.2}$$

where M is given by

$$M = \begin{bmatrix} 1 & S_\phi T_\theta & C_\phi T_\theta \\ 0 & C_\phi & -S_\phi \\ 0 & S_\phi \sec\theta & C_\phi \sec\theta \end{bmatrix}, \tag{2.3}$$

[2]Here, and throughout this paper, for simplicity of notation, we drop the time dependency of the state variables when describing the dynamics

and R can be represented in terms of Euler angles as

$$R = \begin{bmatrix} C_\theta C_\psi & C_\psi S_\theta S_\phi - C_\phi S_\psi & C_\phi C_\psi S_\theta + S_\phi S_\psi \\ C_\theta S_\psi & S_\psi S_\theta S_\phi + C_\phi C_\psi & C_\phi S_\psi S_\theta - S_\phi C_\psi \\ -S_\theta & C_\theta S_\phi & C_\theta S_\phi \end{bmatrix}. \tag{2.4}$$

By substituting the value of ρ from (2.1) to (2.2), we can write

$$\begin{aligned} \dot{x}_\ell &= v_\ell \\ \dot{v}_\ell &= -\frac{T}{m_\ell L}(x_\ell - x_q) - g b_3 \\ \dot{x}_q &= v_q \\ \dot{v}_q &= \frac{u_t}{m_q} R b_3 - g b_3 + \frac{T}{m_q L}(x_\ell - x_q) \\ \dot{\Phi} &= M\Omega \\ \dot{\Omega} &= J^{-1}\left(\tau - (\Omega \times J\Omega)\right). \end{aligned} \tag{2.5}$$

Note that the state vector of the quadrotor system attached with the load has the states $\text{col}(x_\ell, v_\ell, x_q, v_q, \Phi, \Omega) := x := \text{col}(x_1, \cdots, x_{18}) \in \mathbb{R}^{18}$, and the inputs are $\text{col}(\tau_1, \tau_2, \tau_3, u_t) \in \mathbb{R}^4$. We define the position of the point mass (payload) in the inertial frame as the output of (2.5)

$$y = h(x) = x_\ell, \tag{2.6}$$

where $h : \mathbb{R}^{18} \to \mathbb{R}^3$ is a smooth map. A summary of system parameters and states are given in Table 2.1.

3 Problem formulation

Informally, in the path following problem of quadrotor attached with a cable suspended load, the objective is to make the cable suspended load converge to a given path, and then follow it without leaving the path, using the four control inputs of the quadrotor. We highlight the fundamental difference between trajectory tracking and path following, i.e., a trajectory is a time parameterized curve, while a path is considered as a set of points without any notion of time. Let us consider a curve γ, embedded in three-dimensional space, with parameterization

$$\begin{aligned} \sigma : \mathbb{D} &\to \mathbb{R}^3 \\ \lambda &\mapsto \operatorname{col}\left(\sigma_1(\lambda), \sigma_2(\lambda), \sigma_3(\lambda)\right). \end{aligned}$$

Furthermore, we assume that the given curve is regular, i.e., $\|\sigma'(\lambda)\| \neq 0$ for any $\lambda \in \mathbb{D}$. Since any regular curve can be unit speed parameterized by its arc-length [7], we assume, without loss of generality, that the parameterization σ of the curve is a unit speed parameterization, i.e., $\|\sigma'(\lambda)\| = 1$. Similar to [25], we make the following assumption about the curve.

Assumption 2. *The curve $\gamma \subset \mathbb{R}^3$ is one-dimensional embedded sub-manifold. Given any open set W, a smooth map $s : W \subset \mathbb{R}^3 \to \mathbb{R}^2$ exists such that $\gamma = s^{-1}(0)$ with* $\operatorname{rank}(ds_y) = 2$*, for all $y \in \gamma$.*

Since $\gamma = s^{-1}(0)$, for the system (2.5), the path in the output space (2.6) can be represented by its zero-level set representation as

$$\gamma := s^{-1}(0) = \left\{ y \in \mathbb{R}^3 : s_1(y) = s_2(y) = 0 \right\}.$$

Informally, the above assumption restricts the choice of path to non-self intersecting smooth curves.

3.1 Problem statement

Given a quadrotor system attached with a cable suspended load that satisfies Assumption 1 and a regular, embedded C^∞ curve γ satisfying Assumption 2, design, if possible,

a smooth dynamic feedback controller

$$\begin{aligned} \dot{z} &= \mathsf{A}(x,z) + \mathsf{B}(x,z)u \\ \begin{bmatrix} \tau \\ u_t \end{bmatrix} &= \mathsf{C}(x,z) + \mathsf{D}(x,z)u, \end{aligned} \tag{3.1}$$

with $z \in \mathbb{R}^k$, for some $k \in \mathbb{N}$ that needs to be determined, and $u \in \mathbb{R}^4$, such that if the quadrotor attached with the cable suspended load is initialized in an open neighbourhood $\mathcal{U} \times \mathcal{V} \subset \mathbb{R}^{18} \times \mathbb{R}^k$ with $\gamma \subset h(\mathcal{U})$, the system achieves the following objectives:

P1 for each $(x(0), z(0)) \in \mathcal{U} \times \mathcal{V}$, the system converges to the path, i.e., $\|h(x(t))\|_\gamma \to 0$, as $t \to \infty$;

P2 the path $\gamma := s^{-1}(0)$ achieves output invariance, for all $t \geq 0$;

P3 on the path γ, the payload and quadrotor meet additional application-specific requirements such as

- point stabilization of the payload,
- the speed, acceleration or jerk of the payload achieve a desired profile, and
- the heading of the quadrotor satisfies a given reference profile.

4 Dynamic control design

For a quadrotor system attached with load, our objective is to control the position of the payload, i.e, x_ℓ, and also heading of the quadrotor, i.e., ψ. Therefore, we define the augmented-output of (2.5) be

$$\bar{y} := \bar{h}(x_\ell, \psi) = \bar{h}(x_1, x_2, x_3, x_{15}) \in \mathbb{R}^4. \tag{4.1}$$

Next, we demonstrate that the system (2.5) fails to achieve a well-defined vector relative degree for any smooth function of the augmented output space (4.1). To be precise, let $\alpha_i : \mathbb{R}^3 \to \mathbb{R}$, $x_\ell \mapsto \alpha_i(x_\ell)$ for $i \in \{1, 2, 3\}$ be smooth real-valued functions and $\alpha_4 : \mathbb{R}^4 \to \mathbb{R}$, $(x_\ell, \psi) \mapsto \alpha_4(x_\ell, \psi)$ be another smooth real-valued function. To this end, we construct a virtual output function as

$$\bar{y} = \begin{bmatrix} \alpha_1(x_\ell) \\ \alpha_2(x_\ell) \\ \alpha_3(x_\ell) \\ \alpha_4(x_\ell, \psi) \end{bmatrix}. \tag{4.2}$$

The following result shows that there does not exist any smooth function of the form $\bar{y}$ in $\mathbb{R}^4$ that would guarantee a well-defined relative degree of the system.

Lemma 4.0.1. *System (2.5) with the output function (4.2) fails to achieve a well-defined vector relative degree at any $x \in \mathbb{R}^{18}$.*

Proof. Consider system (2.5) and let

$$\bar{f}(x) := \operatorname{col}\Big(v_\ell, -\frac{T}{m_\ell L}(x_\ell - x_q) - gb_3, v_q, \\ -gb_3 + \frac{T}{m_q L}(x_\ell - x_q), M\Omega, J^{-1} - (\Omega \times J\Omega)\Big),$$

$\bar{g}_1(x) := \operatorname{col}\left(0_{15}, \frac{1}{J_x}, 0, 0\right)$, $\bar{g}_2(x) := \operatorname{col}\left(0_{16}, \frac{1}{J_y}, 0\right)$, $\bar{g}_3(x) := \operatorname{col}\left(0_{17}, \frac{1}{J_z}\right)$, and $\bar{g}_4(x) := \operatorname{col}\left(0_9, \frac{1}{m_q} Rb_3, 0_6\right)$, be smooth vector fields on $\mathbb{R}^{18}$. Then, we can express the quadrotor system (2.5) attached with a cable suspended payload in the control-affine form as

$$\dot{x} = \bar{f}(x) + \bar{g}_1(x)\tau_1 + \bar{g}_2(x)\tau_2 + \bar{g}_3(x)\tau_3 + \bar{g}_4(x)u_t.$$

By taking iterative Lie derivative of the functions α_i, for $i \in \{1,2,3\}$, we get

$$L_{\bar{g}_j} L_{\bar{f}}^k \alpha_i = 0, \tag{4.3}$$

for $k \in \{0,\dots,2\}$ and $j \in \{1,\dots,4\}$. Similarly, (4.3) holds true for $j \in \{1,\dots,3\}$ and $k = 3$. The first nonzero Lie derivative appears when we take the fourth derivative along the vector field $\bar{g}_4$, i.e., $L_{\bar{g}_4} L_{\bar{f}}^3 \alpha_i \neq 0$, for $i \in \{1,2,3\}$.

For the function α_4, the first non-zero Lie derivative appears when we take the second derivative along the vector fields $\bar{g}_2$ and $\bar{g}_3$, while the Lie derivatives along the vector fields $\bar{g}_1$ and $\bar{g}_4$ are identically zero. Therefore, the decoupling matrix takes the following form

$$\bar{D}(x) = \begin{bmatrix} 0 & 0 & 0 & L_{\bar{g}_4} L_{\bar{f}}^3 \alpha_1 \\ 0 & 0 & 0 & L_{\bar{g}_4} L_{\bar{f}}^3 \alpha_2 \\ 0 & 0 & 0 & L_{\bar{g}_4} L_{\bar{f}}^3 \alpha_3 \\ 0 & L_{\bar{g}_2} L_{\bar{f}} \alpha_4 & L_{\bar{g}_3} L_{\bar{f}} \alpha_4 & 0 \end{bmatrix}. \tag{4.4}$$

Clearly, $\bar{D}(x)$ is rank deficient for all x in $\mathbb{R}^{18}$ and the system (2.5) fails to exhibit a well-defined vector relative degree. □

On way to interpret the rank deficient decoupling matrix in Lemma 4.0.1 is that the flow of the output vector $\bar{y}$ vanishes along the vector field $\bar{g}_1$. This issue can be resolved by delaying the control input u_t using two integrators, which introduce two additional states $z = \text{col}(z_1, z_2)$. Let $u_t = z_1$, where z_1 is the first state of the dynamic controller. To delay the control input u_t one more time, we select $\dot{z}_1 = z_2$ and $\dot{z}_2 = u_d$, where u_d is the the delayed control input. This leads to the following dynamic controller

$$\begin{aligned} \dot{z}_1 &= z_2 \\ \dot{z}_2 &= u_d. \end{aligned} \tag{4.5}$$

Let $u = \text{col}(u_1, u_2, u_3, u_4) := \text{col}(\tau_1, \tau_2, \tau_3, u_t)$. The augmentation of the two controller states to the system is called dynamic extension and the extended system is given by

$$\begin{aligned} \dot{x}_\ell &= v_\ell \\ \dot{v}_\ell &= -\frac{T}{m_\ell L}(x_\ell - x_q) - g b_3 \\ \dot{x}_q &= v_q \\ \dot{v}_q &= \frac{z_1}{m_q} R b_3 - g b_3 + \frac{T}{m_q L}(x_\ell - x_q) \\ \dot{\Phi} &= M\Omega \\ \dot{\Omega} &= J^{-1}(\tau - (\Omega \times J\Omega)) \\ \dot{z}_1 &= z_2 \\ \dot{z}_2 &= u_d. \end{aligned} \tag{4.6}$$

For notational simplicity, we do not differentiate between the states of system (2.5) and the controller states (4.5), i.e., $(x_1, \ldots, x_{18})$ and (z_1, z_2). Let $x_{19} := z_1$ and $x_{20} := z_2$. Thus, the state vector for the extended system (4.6) is represented by $\mathbf{x} := \text{col}(x_\ell, v_\ell, x_q, v_q, \Phi, \Omega, z_1, z_2) = \text{col}(x_1, \ldots, x_{20}) \in \mathbb{R}^{20}$. For smooth vector fields

$$f(\mathbf{x}) := \text{col}\Bigg(v_\ell, -\frac{T}{m_\ell L}(x_\ell - x_q) - gb_3, v_q, \frac{z_1}{m_q}Rb_3 - gb_3 + \frac{T}{m_q L}(x_\ell - x_q), M\Omega, J^{-1} - (\Omega \times J\Omega), 0, 0\Bigg),$$

$g_1(\mathbf{x}) := \text{col}\left(0_{15}, \frac{1}{J_x}, 0_4\right)$, $g_2(\mathbf{x}) := \text{col}\left(0_{16}, \frac{1}{J_y}, 0_3\right)$, $g_3(\mathbf{x}) := \text{col}\left(0_{17}, \frac{1}{J_z}, 0_2\right)$, and $g_4(\mathbf{x}) := \text{col}\,(0_{19}, 1)$ in $\mathbb{R}^{20}$, the extended system (4.6) can be written in the control-affine form

$$\dot{\mathbf{x}} = f(\mathbf{x}) + \sum_{i=1}^{4} g_i(\mathbf{x})u_i. \tag{4.7}$$

To achieve the objectives **P1** and **P2**, we exploit the zero-level set representation of the given path γ and define

$$\begin{bmatrix} \alpha_1(x) \\ \alpha_2(x) \end{bmatrix} := s \circ h(x) = \begin{bmatrix} s_1 \circ h(x) \\ s_2 \circ h(x) \end{bmatrix}, \tag{4.8}$$

such that $\frac{\partial \alpha_i}{\partial x_j} = 0$, for $i \in \{1, 2\}$, and $j \in \{4, 5, \ldots, 18\}$. Loosely speaking, the maps α_1 and α_2 are solely depended on x_ℓ.

The lift of the given path γ to the state space of the quadrotor attached with the cable suspended load system yields a submanifold of $\mathbb{R}^{20}$, i.e.,

$$\Gamma := \left\{\mathbf{x} \in \mathbb{R}^{20} : s_1(h(x)) = s_2(h(x)) = 0\right\}.$$

When all the states of the system, which include the quadrotor states and the states of the payload, converge to the set Γ, the position of the payload x_ℓ converges to the path γ. However, there is no guarantee that the payload never leaves the path, once all the states of the system (4.6) converge to submanifold Γ. In other words, the lifted path Γ is not an invariant set. Next, we define the path following manifold as an invariant set contained in Γ [10].

Definition 4.0.2. *Given a path γ, the path-following manifold $\Gamma^\star$ of (4.6) is the maximal controlled invariant submanifold contained in the lift of γ. Moreover, $\Gamma^\star$ is a non-empty subset of Γ, with dimension $n^\star \leq 20$.*

The path following manifold can be found by applying the zero dynamics algorithm and is given by

$$\Gamma^\star = \Big\{\mathbf{x} \in \mathbb{R}^{20} : \alpha_1(x) = \ldots = \alpha_1^{(6)}(x) = \alpha_2(x) = \ldots = \alpha_2^{(6)}(x) = 0\Big\}. \tag{4.9}$$

The set $\Gamma^\star$ can be interpreted as an ensemble of all maneuvers of the closed-loop system such that an input signal u can be selected to restrict the evolution of the payload's position to the given path γ. Now, we state two elementary results, which will be used later to prove the main result of this section.

Lemma 4.0.3 ([29]). *For three linearly independent vectors v_1,v_2, and v_3 all in $\mathbb{R}^3$, $\langle v_1, (v_2 \times v_3)\rangle \neq 0$.*

Given σ and α_i defined in Section III and Section IV, respectively, let $d_{x_\ell}\alpha_i := \text{col}(\frac{\partial \alpha_i}{\partial x_1}, \frac{\partial \alpha_i}{\partial x_2}, \frac{\partial \alpha_i}{\partial x_3})$, for $i \in \{1, 2\}$, and let $\sigma' := \text{col}(\frac{\partial \sigma_1}{\partial \lambda}, \frac{\partial \sigma_2}{\partial \lambda}, \frac{\partial \sigma_3}{\partial \lambda})$.

Lemma 4.0.4 ([12]). *Given two smooth maps α_1 and α_2, as defined in (4.8), $\text{span}\{d_{x_\ell}\alpha_1, d_{x_\ell}\alpha_2, \sigma'\} = \mathbb{R}^3$ for all $x_\ell \in \gamma$.*

To achieve **P3**, we invoke the parametric representation σ of the path γ to define another function α_3 in the output space. Consider an open neighbourhood of the curve γ, denoted by $\mathcal{N}(\gamma) \subset \mathbb{R}^3$, such that the following condition is satisfied. Given an element y in the neighbourhood set $\mathcal{N}(\gamma)$, there exists a unique $y^\star \in \gamma$ such that $\|y\|_\gamma = \|y - y^\star\|$. Given such an open set $\mathcal{N}(\gamma)$, we can define the following map:

$$\begin{aligned} \varpi : \mathcal{N}(\gamma) &\to \mathbb{D} \\ y &\mapsto \arg\inf_{\lambda \in \mathbb{D}} \|y - \sigma(\lambda)\|. \end{aligned} \tag{4.10}$$

Using (4.10), the map α_3 is defined as

$$\alpha_3 := \varpi \circ h : \mathbb{R}^{18} \to \mathbb{R}. \tag{4.11}$$

To specify a constraint on the heading of the quadrotor, we can select another function

$$\begin{aligned} \alpha_4 : \mathbb{R}^4 &\to \mathbb{R} \\ (x_\ell, \psi) &\mapsto \alpha_4(x_\ell, \psi), \end{aligned} \tag{4.12}$$

such that α_4 is smooth and $\partial_\psi(\alpha_4) \neq 0$, for all $\mathbf{x} \in \mathbb{R}^{20}$. In summary, given α_1 and α_2 satisfying Lemma 4.0.4, α_3 defined in (4.11), and α_4 defined in (4.12), we construct a refined virtual output function

$$\overline{y} = \begin{bmatrix} \alpha_1(x) \\ \alpha_2(x) \\ \alpha_3(x) \\ \alpha_4(x_\ell, \psi) \end{bmatrix} = \begin{bmatrix} s_1 \circ h(x) \\ s_2 \circ h(x) \\ \varpi \circ h(x) \\ \alpha_4(x_\ell, \psi) \end{bmatrix}. \tag{4.13}$$

Next we determine the vector relative degree of the quadrotor system attached with cable suspended payload.

Theorem 4.0.5. *The extended system (4.7) satisfying* Assumption 1*, with output defined in (4.13), achieves a well-defined vector relative degree of $\{6, 6, 6, 2\}$ everywhere on the set $\Gamma^\star \cap \{\mathbf{x} \in \mathbb{R}^{20} : x_{19} \neq 0, \cos(x_{13}) \neq 0, \cos(x_{14}) \neq 0\}$.*

Proof. Let us consider $x^\star \in \Gamma^\star$ be an arbitrary element and let the path parameter $\lambda^\star \in \mathbb{D}$ be such that $h(x^\star) = \sigma(\lambda^\star)$. By Definition 4.0.2, $\Gamma^\star \subseteq \Gamma$ and it implies that the output $h(x^\star)$ is on the given path γ. By the definition of vector relative degree, we must establish that for each x in a neighbourhood of $x^\star$

$$L_{g_i} L_f^j \alpha_k(x) \equiv 0, L_{g_i}\alpha_4(x) \equiv 0,$$

for $i \in \{1, 2, \ldots, 4\}$, $j \in \{0, \ldots, 4\}$, $k \in \{1, 2, 3\}$ and that the 4×4 decoupling matrix

$$D(x) = \begin{bmatrix} L_{g_1} L_f^5 \alpha_1(x) & \ldots & L_{g_4} L_f^5 \alpha_1(x) \\ L_{g_1} L_f^5 \alpha_2(x) & \ldots & L_{g_4} L_f^5 \alpha_2(x) \\ L_{g_1} L_f^5 \alpha_3(x) & \ldots & L_{g_4} L_f^5 \alpha_3(x) \\ L_{g_1} L_f \alpha_4(x) & \ldots & L_{g_4} L_f \alpha_4(x) \end{bmatrix}, \tag{4.14}$$

is full rank. Direct calculation of Lie derivatives yield

$$L_{g_i} L_f^j \alpha_k(x) = 0, L_{g_i}\alpha_4(x) = 0,$$

for $i \in \{1, 2, 3, 4\}$, and $j \in \{0, \ldots, 4\}$. To show that the decoupling matrix is full rank, we analyze its determinant.

$$\begin{aligned} \det(D(x)) = &\left(\frac{T^3 x_{19}^2 \cos(x_{13})}{\det(J) L^3 m_\ell^3 m_q^3 \cos(x_{14})}\right)(\partial_\psi \alpha_4) \\ &(\partial_{x_1}\alpha_1 (\partial_{x_2}\alpha_2 \sigma_3' - \partial_{x_3}\alpha_2 \sigma_2') + \\ &\partial_{x_2}\alpha_1 (\partial_{x_3}\alpha_2 \sigma_1' - \partial_{x_1}\alpha_2 \sigma_3') + \\ &\partial_{x_3}\alpha_1 (\partial_{x_1}\alpha_2 \sigma_2' - \partial_{x_2}\alpha_2 \sigma_1')), \end{aligned} \tag{4.15}$$

which can be further simplified as

$$\begin{aligned} \det(D(x)) = &\left(\frac{T^3 x_{19}^2 \cos(x_{13})}{\det(J) L^3 m_\ell^3 m_q^3 \cos(x_{14})}\right)(\partial_\psi \alpha_4) \\ &\langle d_{x_\ell}\alpha_1, (d_{x_\ell}\alpha_2 \times \sigma')\rangle. \end{aligned} \tag{4.16}$$

The determinant of the decoupling matrix vanishes whenever any term in the numerator of (4.16) goes to zero or any factor in the denominator is infinity. The determinant of J is finite since all the diagonal terms of the inertia matrix are finite. Moreover, m_q and m_ℓ are the mass of quadrotor and suspended point mass, respectively, which are positive finite constants. The tension in the string T is positive by Assumption 1. The term $\cos(x_{14})$ is bounded and is therefore finite; the physical parameter L, which is the length of cable, is non-zero. By Lemma 4.0.4, the $\text{span}\{d_{x_\ell}\alpha_1, d_{x_\ell}\alpha_2, \sigma'\} = \mathbb{R}^3$. Therefore, by Lemma 4.0.3, the $\langle d_{x_\ell}\alpha_1, (d_{x_\ell}\alpha_2 \times \sigma')\rangle \neq 0$. Also, by definition, $\partial_\psi \alpha_4 \neq 0$. Therefore, we have shown that the determinant of the decoupling matrix is non-zero for all $x^\star \in \Gamma^\star \cap \{\mathbf{x} \in \mathbb{R}^{20} : x_{19} \neq 0, \cos(x_{13}) \neq 0, \cos(x_{14}) \neq 0\}$ and the extended system (4.7) achieves a well defined vector relative degree of $\{6, 6, 6, 2\}$. □

Next we define a coordinate transformation that converts the nonlinear extended system to an exact linear form.

Corollary 4.0.6. *Let $x^\star \in \Gamma^\star \backslash \{\mathbf{x} \in \mathbb{R}^{20} : x_{13} = x_{14} = \pm\pi/2, x_{19} = 0\}$. There exists a neighbourhood $U \subset \mathbb{R}^{20}$ containing $x^\star$ such that the mapping $\mathscr{T} : U \subset \mathbb{R}^{20} \to \mathscr{T}(U) \subset \mathbb{R}^{20}$, defined by*

$$\begin{bmatrix} \xi_i \\ \zeta_i \\ \eta_i \\ \mu_j \end{bmatrix} = \mathscr{T}(x) = \begin{bmatrix} L_f^{i-1}\alpha_1(x) \\ L_f^{i-1}\alpha_2(x) \\ L_f^{i-1}\alpha_3(x) \\ L_f^{j-1}\alpha_4(x) \end{bmatrix}, \tag{4.17}$$

for $i \in \{1, \ldots, 6\}$ and $j \in \{1, 2\}$ is a diffeomorphism.

Proof. The choice of the coordinates $(\xi, \zeta, \eta, \mu) \in \mathbb{R}^{20}$ is clear from (4.17). Next we need to check the rank of the 20×20 Jacobian matrix of the coordinate transformation $\mathscr{T}$. The determinant of the Jacobian matrix simplifies to

$$\begin{aligned} \det(d\mathscr{T}_{x^\star}) = &\left(\frac{T^{12} x_{19}^4 \cos^2(x_{13})}{L^{12} m_\ell^{12} m_q^6 \cos(x_{14})} \right) (\partial_\psi \alpha_4)^2 \\ &\left(\langle d_{x_\ell} \alpha_1, (d_{x_\ell} \alpha_2 \times \sigma') \rangle \right)^6 \Big|_{x^\star}, \end{aligned} \tag{4.18}$$

which can be easily justified to be non-zero by using arguments similar to that used in the proof of Theorem 4.0.5. The inverse function theorem [30, Theorem 5.23] implies that the coordinate transformation $\mathscr{T}$ is a diffeomorphism onto its image. □

The diffeomorphism $\mathscr{T}$ from Corollary 4.0.6 allows us to the express the system in term

of transformed states $(\xi, \zeta, \eta, \mu) \in \mathbb{R}^{20}$, i.e.,

$$\begin{aligned}
\dot{\xi}_1 &= \xi_2 \\
&\vdots \\
\dot{\xi}_5 &= \xi_6 \\
\dot{\xi}_6 &= L_f^6 \alpha_1 + \sum_{i=1}^{4} L_{g_i} L_f^5 \alpha_1 u_i \Big|_{x=\mathscr{T}^{-1}(\xi,\zeta,\eta,\mu)} \\
\dot{\zeta}_1 &= \zeta_2 \\
&\vdots \\
\dot{\zeta}_5 &= \zeta_6 \\
\dot{\zeta}_6 &= L_f^6 \alpha_2 + \sum_{i=1}^{4} L_{g_i} L_f^5 \alpha_2 u_i \Big|_{x=\mathscr{T}^{-1}(\xi,\zeta,\eta,\mu)} \\
\dot{\eta}_1 &= \eta_2 \\
&\vdots \\
\dot{\eta}_5 &= \eta_6 \\
\dot{\eta}_6 &= L_f^6 \alpha_3 + \sum_{i=1}^{4} L_{g_i} L_f^5 \alpha_3 u_i \Big|_{x=\mathscr{T}^{-1}(\xi,\zeta,\eta,\mu)} \\
\dot{\mu}_1 &= \mu_2 \\
\dot{\mu}_2 &= L_f^2 \alpha_4 + \sum_{i=1}^{4} L_{g_i} L_f \alpha_4 u_i \Big|_{x=\mathscr{T}^{-1}(\xi,\zeta,\eta,\mu)} .
\end{aligned} \tag{4.19}$$

This coordinate transformation suggests a natural choice of feedback transformation

$$\begin{bmatrix} u_1 \\ u_2 \\ u_3 \\ u_4 \end{bmatrix} := D^{-1}(x) \left(\begin{bmatrix} -L_f^6 \alpha_1 \\ -L_f^6 \alpha_2 \\ -L_f^6 \alpha_3 \\ -L_f^2 \alpha_4 \end{bmatrix} + \begin{bmatrix} v^\xi \\ v^\zeta \\ v^\eta \\ v^\mu \end{bmatrix} \right), \tag{4.20}$$

where $(v^\xi, v^\zeta, v^\eta, v^\mu)$ are auxiliary control inputs. By Theorem 4.0.5, this controller (4.20) is well-defined in a neighbourhood of every $x^\star \in \Gamma \backslash \{\mathbf{x} \in \mathbb{R}^{20} : x_{13} = x_{14} = \pm 90^\circ\}$. This means that in a neighbourhood of the path γ, the quadrotor system with the cable suspended payload (4.6) is reduced to four decoupled chain of integrators.

$$\begin{aligned}
&\dot{\xi}_1 = \xi_2 \quad \dot{\zeta}_1 = \zeta_2 \quad \dot{\eta}_1 = \eta_2 \quad \dot{\mu}_1 = \mu_2 \\
&\dot{\xi}_2 = \xi_3 \quad \dot{\zeta}_2 = \zeta_3 \quad \dot{\eta}_2 = \eta_3 \quad \dot{\mu}_2 = v^\mu. \\
&\quad \vdots \qquad\quad \vdots \qquad\quad \vdots \\
&\dot{\xi}_6 = v^\xi \quad \dot{\zeta}_6 = v^\zeta \quad \dot{\eta}_6 = v^\eta
\end{aligned} \tag{4.21}$$

The above system consists of four decoupled linear time invariant (LTI) systems and any linear control technique can be used to stabilize (4.21). We call the first chain of integrators ξ-subsystem, the second chain of integrators ζ-subsystem, the third chain of integrators η-subsystem and fourth chain of integrators μ-subsystem. The output (4.13) is a flat output [31] for the quadrotor system with a load (4.6) because these outputs transform the system to a fully linear system. The linear form of the system in the transformed coordinates simplifies the design of path following controllers.

4.1 Auxiliary controller design

In the previous section, we showed that the quadrotor system with the cable suspended payload (4.6) is geometrically equivalent to the chain of integrators (4.21) via the coordinate and feedback transformations (4.17), (4.20). This geometric equivalence significantly simplifies the controller design process, as the chain of integrators in (4.21) can be controlled using elementary linear control techniques. It is intuitive to see that, in order to bring the system on the set Γ, we exponentially stabilize ξ- and ζ-subsystem by the following controllers:

$$v^{\xi} = \sum_{i=1}^{6} k_i^{\xi} \xi_i, \tag{4.22}$$

$$v^{\zeta} = \sum_{i=1}^{6} k_i^{\zeta} \zeta_i, \tag{4.23}$$

with appropriate values of gains k_i^{ξ}, and k_i^{ζ}, which can be determined by pole placement or similar other LTI system techniques. When all the ξ and ζ states are zero, the system converges to the path, i.e., **P1** and **P2** are satisfied and path invariance is achieved.

To fulfill the objective of making the cable suspended load stop along the path, controlling the speed of the suspended load along the curve, and forcing the cable suspended load to follow a given acceleration profile, jerk and high derivatives along the curve, we design the linear controller of the form

$$v^{\eta} = \sum_{i=1}^{6} k_i^{\eta} (\eta_i - \eta_i^{ref}), \tag{4.24}$$

where the gain k_i^{η} can be determined using pole placement or similar linear control techniques.

It should be noted that η_1 specifies the position of the payload along the path. By selecting η_1^{ref} as the target value, point stabilization of the suspended load along the path is achieved. By setting $k_1^{\eta} = 0$, and selecting η_2^{ref} as the target velocity profile, the suspended load follows the desired profile along the curve. Similarly, by selecting $k_1^{\eta} = k_2^{\eta} = 0$, and setting η_3^{ref} to the reference acceleration profile, the suspended

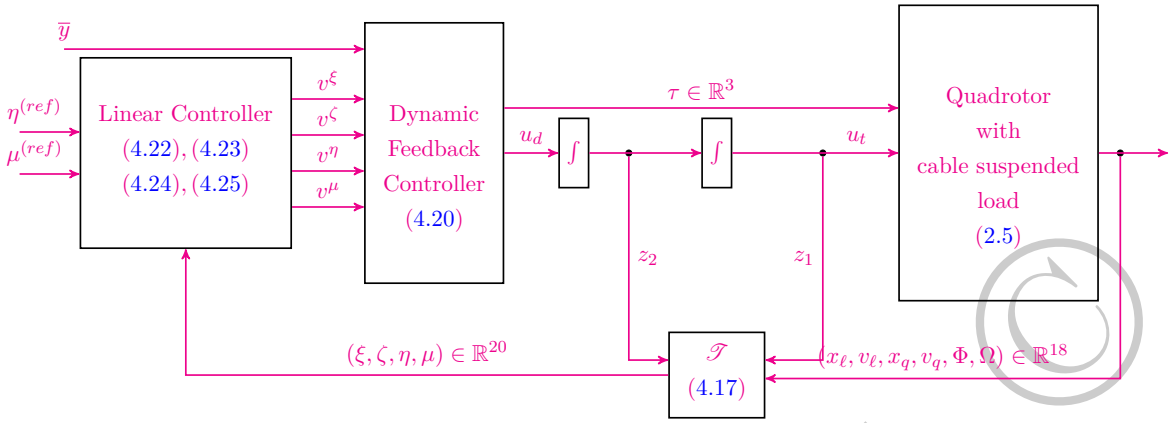

Figure 4.1: The overall system architecture for the proposed controller design is shown. The feedback block transforms the non-linear dynamics to an exact linear form. The outputs of the linear controller are fed into the dynamic feedback controller block that computes the control inputs for the system.

payload follows the desired profile. In other words, the linear controller given by (4.24) satisfies **P3**.

The heading angle of the quadrotor ψ can be controlled by designing a similar linear controller for the μ-subsystem

$$v^\mu = k_1^\mu(\mu_1 - \mu_1^{ref}) + k_2^\mu \mu_2, \tag{4.25}$$

where the gains can be selected using linear control techniques. This controller allows to achieve a given reference profile for the yaw angle, and as a consequence the closed loop system achieves objective **P3**. In summary, the coordinate and feedback transformations (4.17), (4.20) convert the system (4.6) into an exact linear form, and the auxiliary linear controllers (4.22), (4.23), (4.24), and (4.25) satisfy **P1-P3**, and hence, path following problem is solved. The overall control scheme is shown in Figure 4.1.

4.2 Simulation results

In this section, we present simulation results of the quadrotor system attached with a cable suspended payload for two scenarios. First, we present the case when the task is to follow a given closed path. Next, we investigate the case when the system is required to follow a non-closed curve in the presence of parametric uncertainties and sensor noise.

4.3 Path following of a closed curve

The goal is to make the suspended load follow the given parametric curve

$$\sigma \mapsto \text{col}(4\cos(\lambda), 4\sin(\lambda), 10 + \sin(\lambda)).$$

In other words, the target is to make the cable suspended load converge and follow the following path

$$\overline{y} = \begin{bmatrix} x_1^2 + x_2^2 - 16 \\ x_3 - 10 + \sin\left(\tan^{-1}(\frac{x_2}{x_1})\right) \\ \tan^{-1}(\frac{x_2}{x_1}) \\ x_{15} - \frac{\pi}{4} \end{bmatrix}. \tag{4.26}$$

The path following maneuver is shown in Figure 4.2. The desired path γ is shown

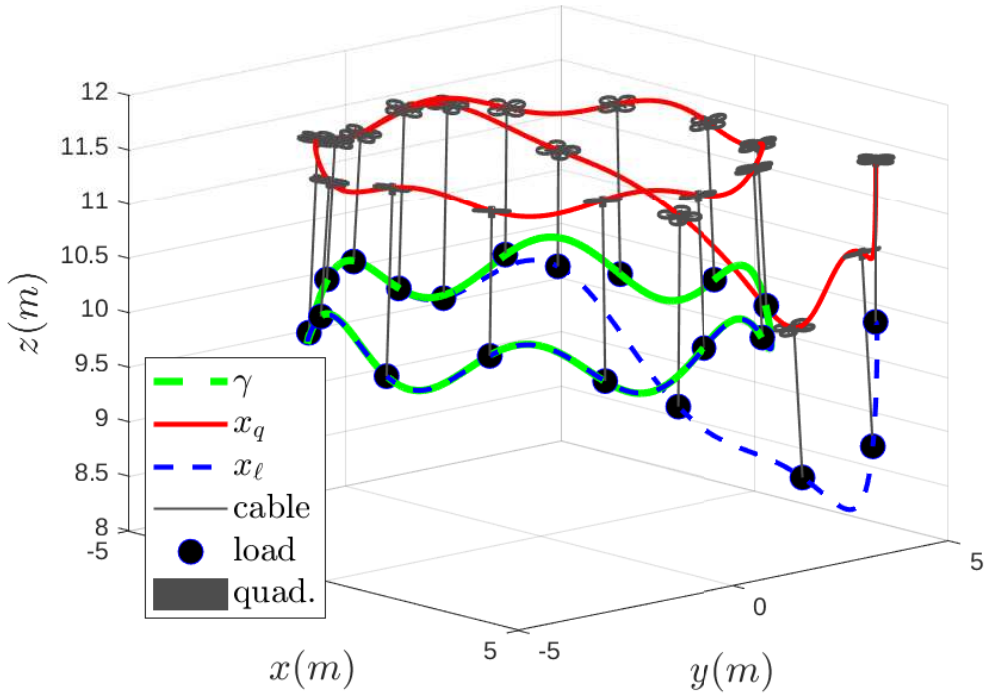

Figure 4.2: The three-dimensional position of the quadrotor and the cable-suspended load is shown in the output space. A system schematic has been overlayed on the curves traced by the load and the quadrotor at periodic intervals in time. The system was initialized away from the path, then it converged to the assigned path and subsequently maintained itself on the path.

by the dotted green line and the path traversed by the load is shown by the solid blue line. The path traversed by the quadrotor for this mission is shown by a solid red line.

Figure 4.2 shows the time snapshots of the quadrotor with the cable suspended load at every second. The cable is represented by the grey line and the load is represented by a solid black blob. As seen in the figure, the system is initialized away from the desired path, i.e., $x_\ell(0) = \text{col}(5, 5, 10)$, and the controllers (4.22) and (4.23) force the load to converge to the desired path. Specifically, not only, the load converges to the set Γ, but it converges to $\Gamma^\star$. Since, $\Gamma^\star$ is invariant, the load never leaves the set, i.e., the load stays on the path for all future time. Another way to interpret the stability of the set $\Gamma^\star$ is to investigate the state trajectories of the ξ- and ζ-subsystem. As seen in Figure 4.3, all the ξ and ζ states converge to zero, i.e., the suspended payload converges to the path, and it stays on the path for all time. The motion along the path is governed by the

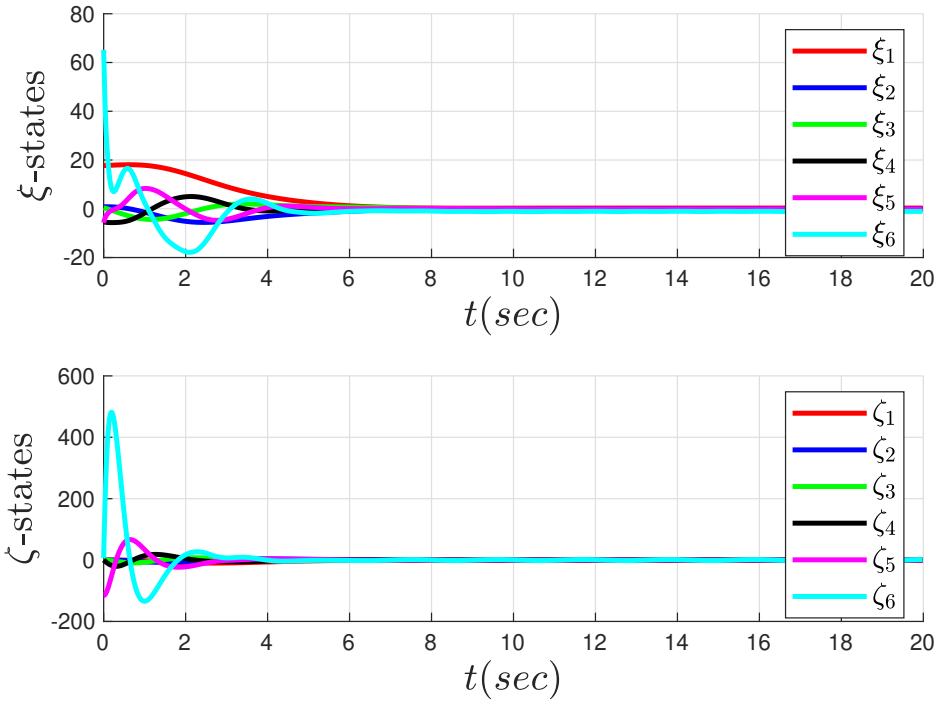

Figure 4.3: Trajectories of ξ and ζ states. The state ξ_1 is the distance from the desired path in the xy-plane. The states ξ_2,ξ_3,...,ξ_6 represents the first derivative of ξ_1,ξ_2,...,ξ_5, respectively. The state ζ_1 is the distance of the load from the desired path along the z-axis. Similarly, the states ζ_2,ζ_3,...,ζ_6 represents the first derivative of ζ_1,ζ_2,...,ζ_5, respectively.

η-subsystem. The goal in this simulation is to follow the desired path with a constant angular velocity of 0.5 rad/secs in the counter clockwise direction, i.e. $\eta_2 - 0.5 = 0$. By applying the controller (4.24), it can be seen in the top plot of Figure 4.4 that η_2 converges to the desired speed of 0.5 rad/secs. This makes η_1 evolve freely, while the states $\eta_3, \ldots, \eta_6$ converge to zero, as shown in Figure 4.4. The heading of the quadrotor is forced to converge to the desired heading value by the controller (4.25). As seen in the

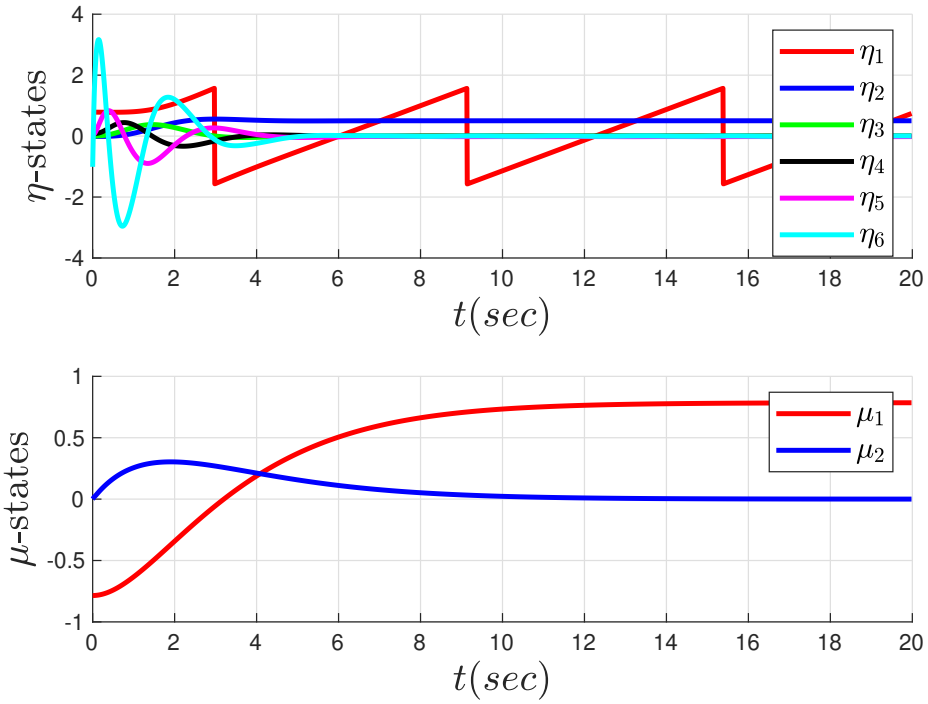

Figure 4.4: Trajectories of η and μ states are shown in the figure. The state η_1 is the position of the load along the desired curve. The states η_2,η_3,...,ξ_5 represent the velocity, acceleration, and higher derivatives, respectively. μ_1 represents the yaw-angle of the quadrotor, while μ_2 represents the derivative of the yaw-angle.

bottom plot of Figure 4.4, the first μ-state converges to the desired value of $\pi/4$, while μ_2 converges to zero. Finally, in Figure 5.7 control inputs are shown. It can be seen in the figure that, on average, 11.5 N of thrust force is required to hover the system. Initially, a larger control effort can be observed in the body torques, which is needed to bring the system to the desired height and the desired path. However, as shown in the figure, even the initial torques are within the actuation limits. Cable tension over the period of time is shown in Figure 4.6. It can be seen that the oscillations in the cable tension correspond to changing height profile of the given path as the quadrotor moves up along the curve, the cable tension increases, and vice versa.

4.4 Path following of a non-closed curve with noise

In this subsection, we consider the path following problem for the quadrotor tethered to a load in a practical scenario. The imperfections in a practical situation are modeled by the presence of Gaussian noise in sensing the state and the uncertainties in the system parameters. We assume 1% of parametric uncertainties for m_q, m_ℓ, and L

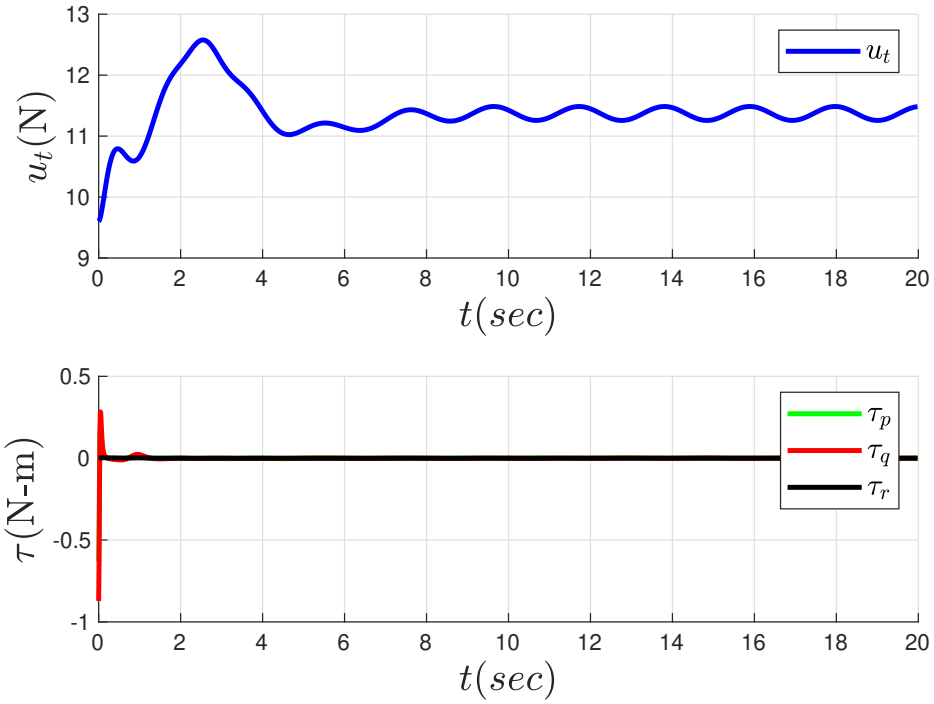

Figure 4.5: Control inputs, i.e., thrust and the body torques, are plotted for a closed path following scenario. It can be observed that the control inputs do not exceed the actuation limits of the plant.

as these parameters can be precisely measured. However, we assume 10% parametric uncertainties for the inertia matrix of the quadrotor, as it is difficult to measure the inertia matrix accurately. We assume that quadrotor is equipped with a standard inertial measurement unit (IMU), such as the one equipped on AscTech Pelican quadrotor, and the on-board computer gives measurements of angles of the quadrotor and body rates. Moreover, we assume that the quadrotor is operating in an indoor arena equipped with Vicon motion capture system which can measure position and velocity of the load and quadrotor. We simulate the system under practical noise level for these sensors, for details see [32].

In the presence of uncertainties and sensor noise, as mentioned above, the task is to make the cable-suspended load follow the non-closed curve

$$\lambda \mapsto \text{col}(\lambda, \sin(\lambda), 10).$$

In other words, the target is to make the cable suspended load converge and follow the

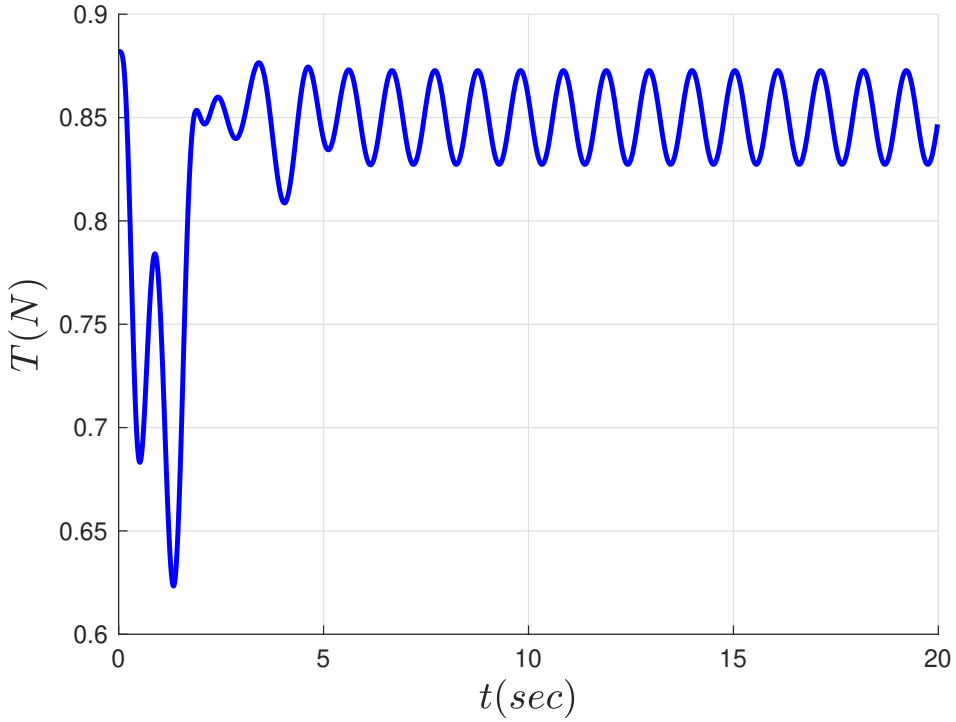

Figure 4.6: Cable tension is plotted as a function of time during the flight of the quadrotor and the cable-suspended load. It can be observed that the tension varies as the quadrotor adjusts its height to keep the load onto the assigned path.

path

$$\overline{y} = \begin{bmatrix} x_2 - \sin x_1 \\ x_3 - 10 \\ x_1 \\ x_{15} - \frac{\pi}{4} \end{bmatrix}. \tag{4.27}$$

The system is initialized at a challenging initial position of $x_\ell(0) = \text{col}(0, -10.1, 10)$, and as shown in Figure 4.7, the load converges to the path. It can be seen in the figure that the quadrotor undergoes large rotations about the roll and pitch axis to make the load converge to the desired path γ and then forces the load to stay on the desired path. Figure 4.8 shows that both ξ- and ζ states converge to zero, i.e., the path following manifold $\Gamma^\star$ achieves stability. We conclude this section by presenting the state trajectory plots of the η- and μ-subsystem. As seen in the top plot of Figure 4.9, η_2 converges to the desired value, while η_1 is evolving freely. The rest of the η states get close to zero. The convergence of η_6 is more sensitive to noise due to the sixth-order derivative of the position of the load. We want to highlight that irrespective of the noise levels in η_6, the load precisely follows the path. Similarly, in the bottom plot of Figure 4.9, the state μ_1 converges to the desired heading value, and μ_2 converges to

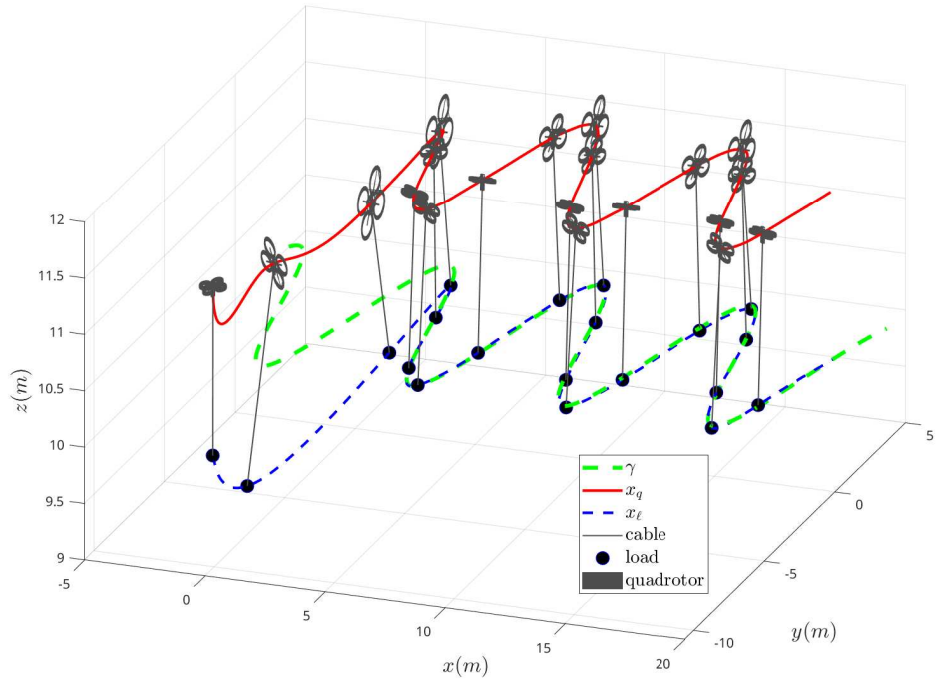

Figure 4.7: The three-dimensional position of the quadrotor and the cable-suspended load is shown in the output space for a non-closed path. A system schematic has been overlayed on the curves traced by the load and the quadrotor at periodic intervals in time. The system was initialized away from the path, then it converged to the assigned path and subsequently maintained itself on the path.

zero.

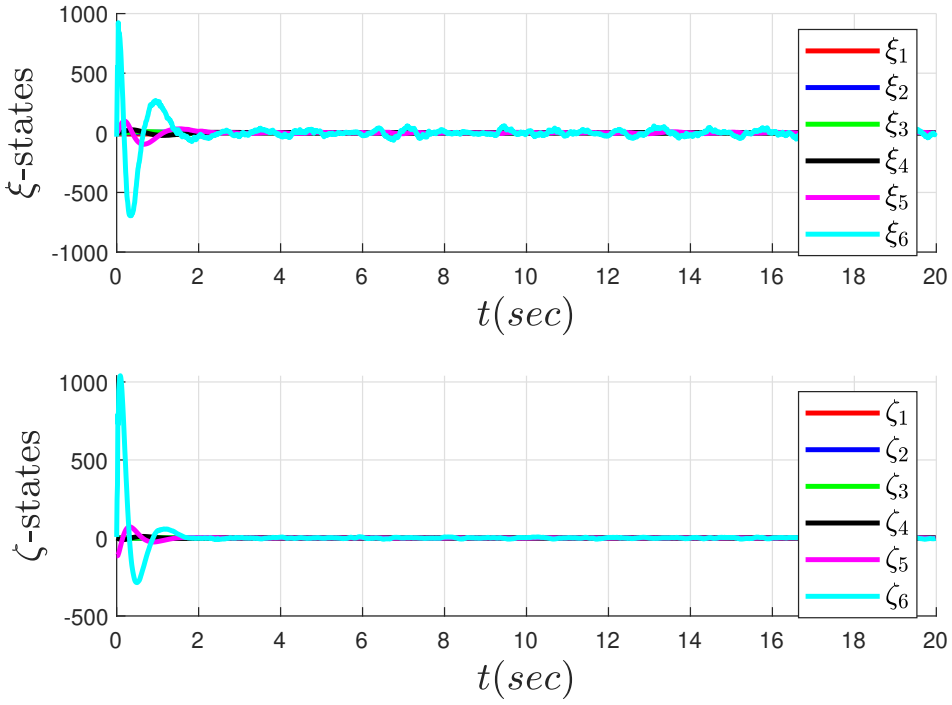

Figure 4.8: Trajectories of ξ and ζ states in the presence of sensor noise and parametric uncertainties are shown in the figure. The state ξ_1 is the distance from the desired path in the xy-plane. The states ξ_2,ξ_3,...,ξ_6 represents the first derivative of ξ_1,ξ_2,...,ξ_5, respectively. The state ζ_1 is the distance of the load from the desired path along the z-axis. Similarly, the states ζ_2,ζ_3,...,ζ_6 represents the first derivative of ζ_1,ζ_2,...,ζ_5, respectively.

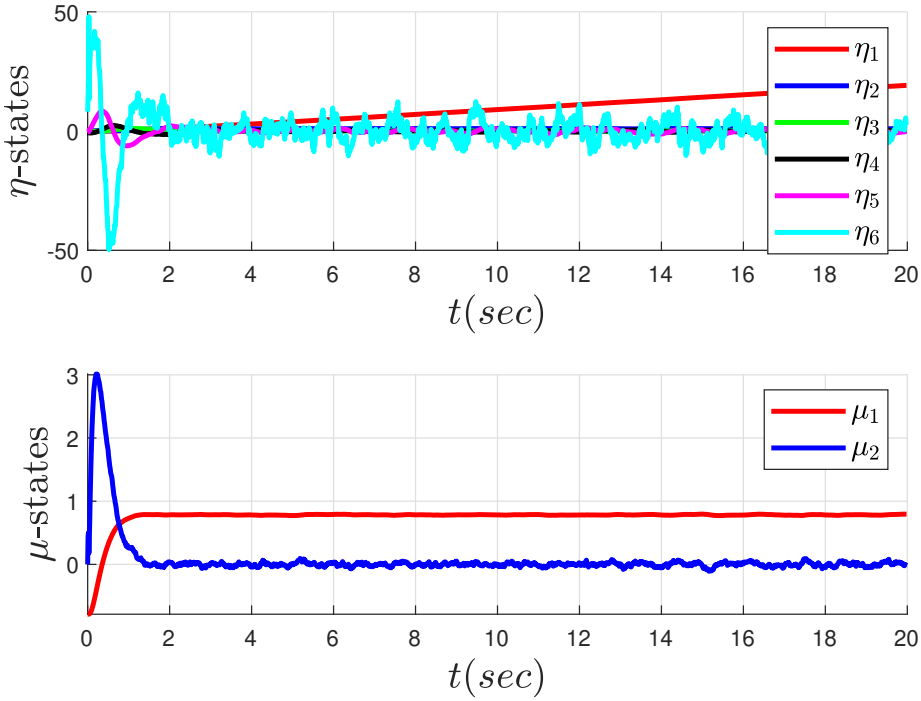

Figure 4.9: Trajectories of η and μ states in the presence of sensor noise and parametric uncertainties when following a non-closed curve. The state η_1 is the position of the load along the desired curve. The states η_2,η_3,...,ξ_5 represent the velocity, acceleration, and higher derivatives, respectively. μ_1 represents the yaw-angle of the quadrotor, while μ_2 represents the derivative of the yaw-angle.

5 Experimental results

In this section, we first discuss the experimental setup along with details of the hardware implementation of the proposed controller. Finally, we demonstrate successful real-world experimental validation of the proposed controller on a Quanser QDrone[1] quadrotor system with a cable suspended payload.

5.1 Experimental setup

The experimental setup consists of a flying arena, a camera system, a UAV with a cable suspended load, a ground station, and a WiFi router, as shown in Figure 5.1. The flying arena has dimensions given by 10m $\times$ 6m $\times$ 11m and is equipped with 16 Natural Point Optitrack Flex-13 cameras that cover the whole space. The Optitrack camera system, as shown in Figure 5.1, is connected to a ground station via high-speed USB cables. Moreover, to ensure human safety, the arena is surrounded by a protective net, and protective floor tiles ensure drone safety. The UAV used in this experimental work is a drone manufactured by Quanser, called QDrone. The Quanser QDrone autonomous air vehicle is a mid-sized quadrotor equipped with a powerful on-board Intel® Aero Compute Board (powered by a quad-core Intel Atom® processor) Quad-core 64-bit 2.56 GHz processor 4 GB LP-DDR3-1600 RAM, and a custom impact-resistant carbon fiber frame. The dimensions of QDrone are 40 $\times$ 40 $\times$ 15 cm, and it weighs around 850 g with batteries. The maximum payload capacity of QDrone is 300g. QDrones are equipped with four high-speed Electronic Speed Controlled (ESC) brushless motors with Hall-effect sensor outputs. The drone has a 3-axis 16-bit accelerometer, range configurable for $\pm$2g to $\pm$16g, a 3-axis gyroscope, range configurable for $\pm$125 deg/s to $\pm$2000 deg/s, and a 3-axis magnetometer. Infra-Red (IR) markers are attached with QDrone, and the cable-suspended load to get tracked by the camera system, as shown in Figure 5.2.

The data stream coming from all 16 cameras is fed into the software, Motive, that comes with the camera system. The motive software runs an optimization algorithm and calculates an accurate pose of the system, which consists of a quadrotor and a cable suspended load at 100 Hz. The pose information provided by the motive software

[1] https://www.quanser.com/products/qdrone/

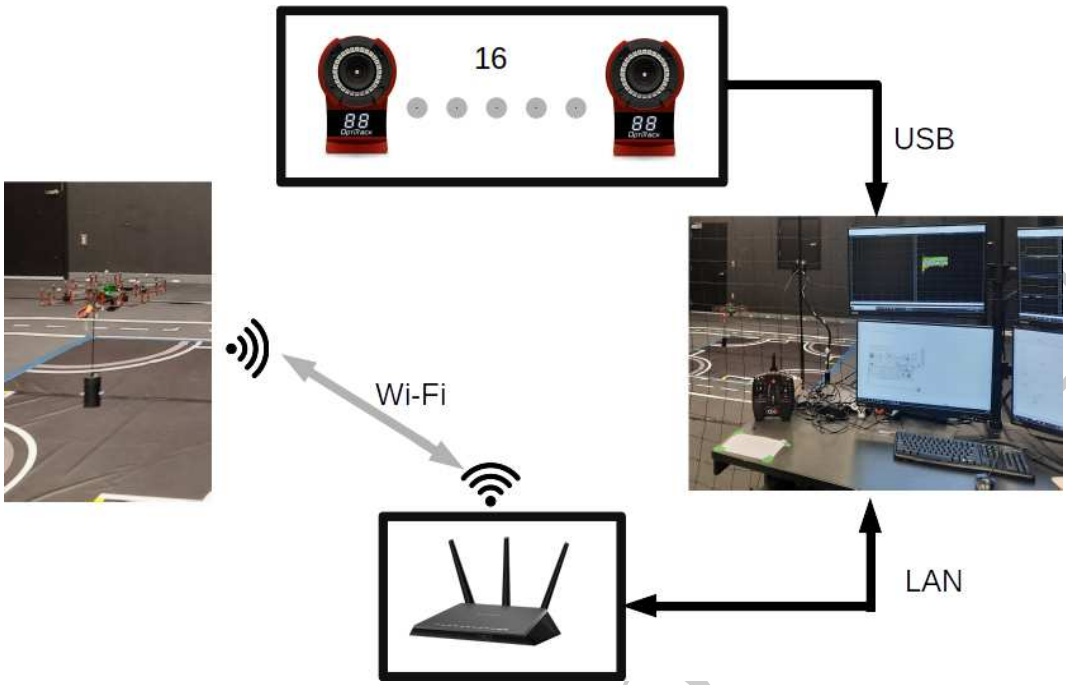

Figure 5.1: An experimental setup based on the Quanser QDrone system is shown in the figure. The overall design consists of 16 cameras, as shown in the top bock; a ground station, as shown in the right bock; a WiFi router, shown in the bottom block; and QDrone during flight with a cable-suspended payload, as shown in the left block.

consists of the three-dimensional position of the quadrotor and load and the orientation of the quadrotor. This information is sent to the onboard controller mounted on the quadrotor via a high-speed WiFi link. Opti-track data and the IMU-sensor data are fused together using vendor-provided complementary filter modules. Moreover, using Hall-effect sensors, motor speed and thrust is measured. In summary, at this point, the system makes all the required state information available at 100 Hz.

5.2 Hardware Implementation

Before presenting the experimental results, we enlist relevant system parameters in Table 5.1. In this experiment, the assigned path to be followed by the load is a unit circle at the height of 0.3 meters with a center coinciding with the center of the arena. At the outset of the experiment, both the quadrotor and the cable are lying on the ground. The tension in the cable at this stage is zero. Therefore, the quadrotor initializes in a mode that takes it off to a height such that it hovers with load hanging above the ground. In this way, before the controller is invoked, it is ensured the tension in the string is non-zero (Assumption 1), and the swing in the load is sufficiently damped. The position of the load and the quadrotor is shown in Figure 5.3 throughout the duration of the flight using blue and red colored curves, respectively. The initial position of

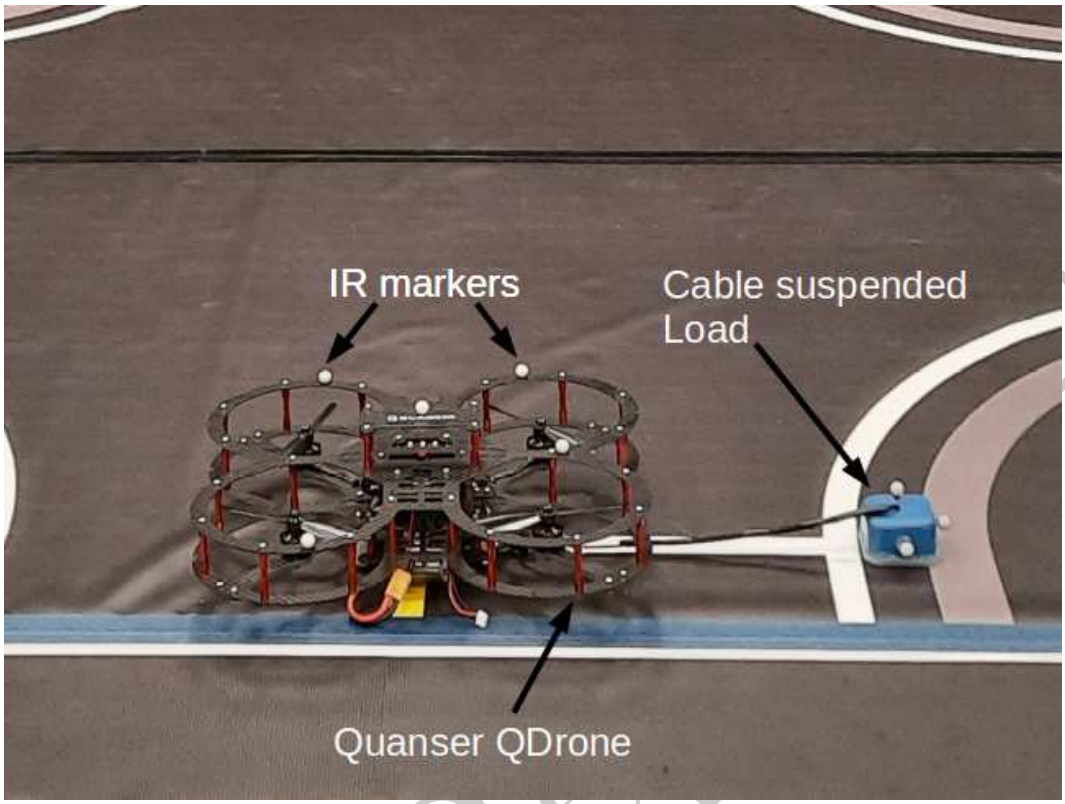

Figure 5.2: QDrone with cable-suspended load is shown in the figure. The IR markers are attached to both the quadrotor and the cable-suspended load to get tracked by the Optitrack camera system.

the two rigid bodies, i.e., the load and the quadrotor, on the ground are indicated by markers in the figure. Once the quadrotor starts hovering and the load swing is reasonably reduced, the proposed controller is invoked, and the load starts approaching and traversing along the assigned circular path. The gains of the controller are carefully designed using classical pole-placement techniques and further refined by tuning. These gains are shown in Table 5.2. At the termination of the mission, the autonomous landing mode of the quadrotor is activated. This results in both the load and the quadrotor safely land on the ground.

Due to the sensor noise and small errors involved in state estimation, an error could be introduced in the position of the load with reference to the assigned path. For the experiment under discussion, the position error in the x-y plane is plotted in Figure 5.4, and the error in the height of the load is shown in Figure 5.5. As shown in Figure 5.4 and Figure 5.5, the initial error is large as the QDrone prepares for the mission. The error starts reducing as the controller is invoked around 7 seconds after the start of the experiment. In the steady-state, the system performs very well as the magnitudes of the position errors are small even in the presence of latency and noise, as shown in

Table 5.1: Parameters of QDrone and cable suspended load

Description	Physical value
cable length L	0.4 m
mass of the quadrotor m_q	0.85 kg
mass of the payload m_ℓ	0.13 kg
inertia of the quadrotor $J = \text{diag}(J_x, J_y, J_z)$	(0.01,0.0082,0.0148) kg.m^2
maximum payload capacity	0.3 kg

Table 5.2: Controller gains

Description	Symbols	Values
ξ-system gains (4.22)	$\left\{k_1^\xi, k_2^\xi, k_3^\xi, k_4^\xi, k_5^\xi, k_6^\xi\right\}$	$\{41.0473, 133.8854, 181.2496, 130.3594, 52.5375, 11.2500\}$
ζ-system gains (4.23)	$\left\{k_1^\zeta, k_2^\zeta, k_3^\zeta, k_4^\zeta, k_5^\zeta, k_6^\zeta\right\}$	$\{41.0473, 133.8854, 181.2496, 130.3594, 52.5375, 11.2500\}$
η-system gains (4.24)	$\{k_1^\eta, k_2^\eta, k_3^\eta, k_4^\eta, k_5^\eta, k_6^\eta\}$	$\{0.0, 43.8716, 74.2399 \; 66.7440, 33.6240, 9.0000\}$
μ-system gains (4.25)	$\{k_1^\mu, k_2^\mu\}$	$\{0.2750, 1.0500\}$

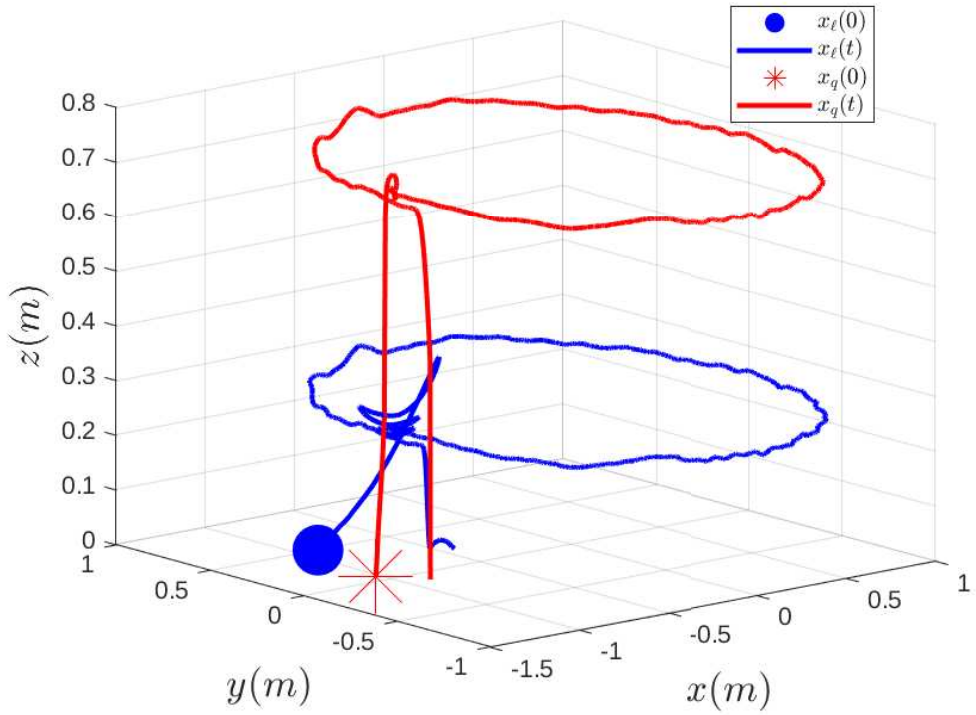

Figure 5.3: Position of the suspended load and the Quanser QDrone in a three-dimensional arena. The initial position of the load and the quadrotor are indicated by markers. The circular path followed by the load is also shown.

Figure 5.4 and Figure 5.5.

Finally, we show the control effort, i.e., total thrust u_t and body torques τ, generated by QDrone in Figure 5.6 and Figure 5.7, respectively. It can be seen that the control effort generated by the system corresponds to the overall inertia of the drone and the mass of the suspended load. Also, the control effort indicates that the controller can successfully stabilize the path following manifold without exceeding the actuation limits of the QDrone system, i.e., 16 N thrust limit and 0.8 N-m body torques limit. Note that in all experimental results reported in this section, the presented figures contain valid data once the controller is invoked (around 7 sec). The overall system works in the hover mode (i.e., the tension in the cable is non-zero). As seen in Figure 5.7, the control torque τ_r is relatively smaller compared to τ_p and τ_q because the quadrotor pose is commanded to a constant value. In contrast, the quadrotor needs to produce small movements in the roll and pitch axis to follow the given circular path.

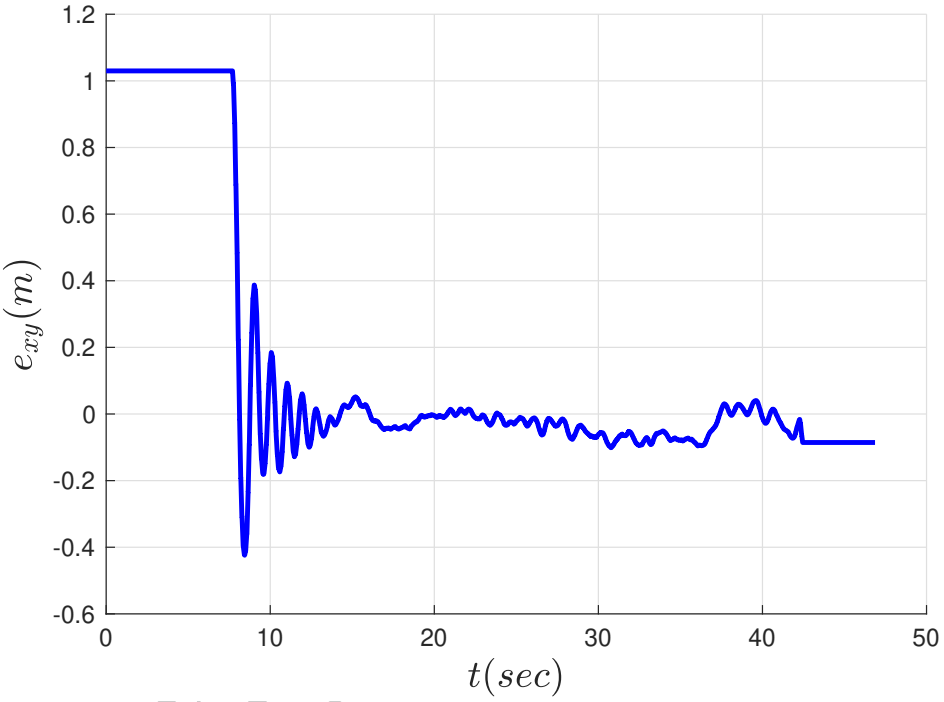

Figure 5.4: Path following error in xy-direction is shown in the figure. This error indicates the difference between the assigned path and the actual position of the load in the x-y plane. The initial error is large when the QDrone is hovering above the ground, and the error reduces in magnitude as the controller takes over. The sign of the error indicates whether the load is inside or outside the assigned path.

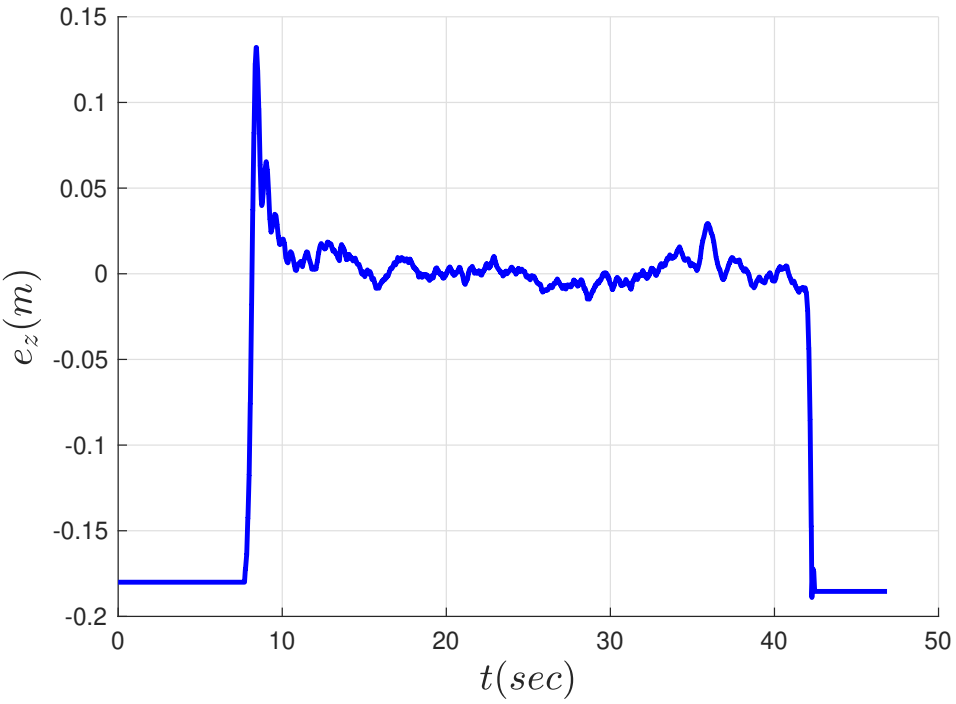

Figure 5.5: Path following error in the z direction is shown in the figure. The error indicates the difference in the assigned path and the height of the load. The controller reduces the initial error in height, and the load approaches the path and follows it.

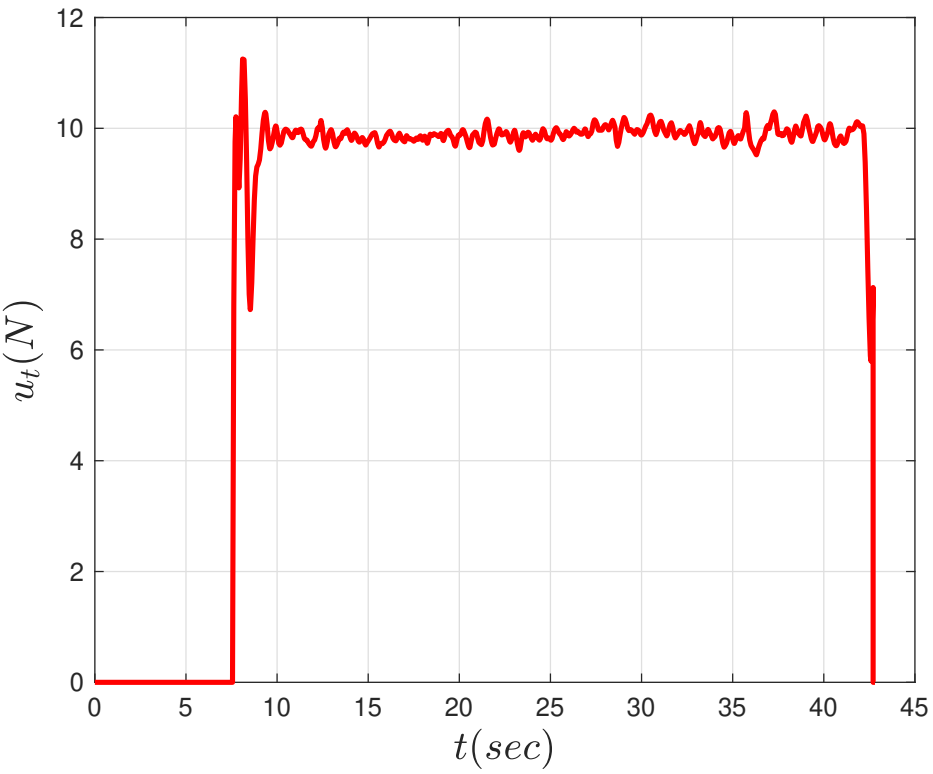

Figure 5.6: Thrust control input u_t generated by the QDrone while following a circular path with a cable suspended load.

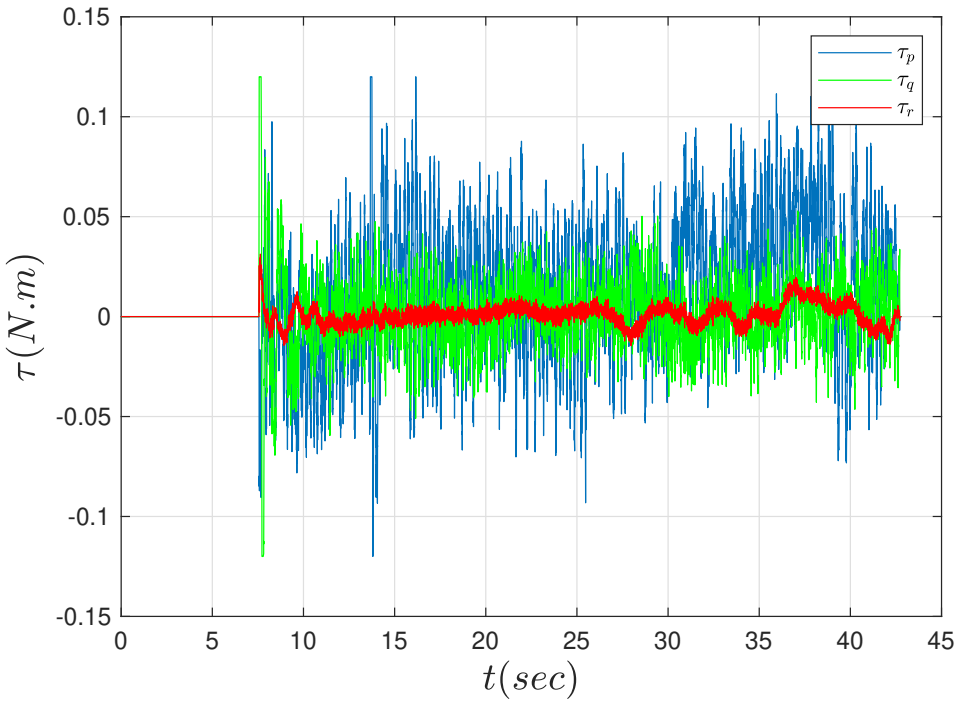

Figure 5.7: Control torques τ_p, τ_q, τ_r generated by the QDrone UAV to make the cable suspended load follow the given circular path. It can be seen that the control efforts are well within the saturation bounds.

6 Conclusion

This paper considers the path following problem for a quadrotor tethered to a load through an inelastic cable. We identify a class of all smooth functions in the output space that ensures the system exhibits a well-defined vector relative degree. A novel smooth dynamic feedback controller is proposed for a large class of both closed and non-closed curves. The proposed controller offers three distinct features: a) the load convergence to the desired path and path invariance; b) the desired motion of the load along the path, which involves point stabilization on the path, following a desired velocity or acceleration profile along the path; c) maintaining a desired orientation of the quadrotor throughout the mission. Simulation results demonstrate the performance of the proposed controllers in the presence of noise and modeling uncertainties. Moreover, successful real-world experimental validation of the proposed controller is demonstrated on a Quanser QDrone UAV platform with a cable-suspended payload.

Bibliography

[1] D. Cabecinhas, R. Naldi, L. Marconi, C. Silvestre, and R. Cunha, "Robust take-off for a quadrotor vehicle," *IEEE Transactions on Robotics*, vol. 28, no. 3, pp. 734–742, June 2012.

[2] S. Yang and B. Xian, "Exponential regulation control of a quadrotor unmanned aerial vehicle with a suspended payload," *IEEE Transactions on Control Systems Technology*, pp. 1–8, 2019.

[3] S. Thapa, H. Bail, and J. A. Acosta, "Cooperative aerial load transport with attitude stabilization," in *2019 American Control Conference (ACC)*, July 2019, pp. 2245–2250.

[4] D. Zhou, Z. Wang, and M. Schwager, "Agile coordination and assistive collision avoidance for quadrotor swarms using virtual structures," *IEEE Transactions on Robotics*, vol. 34, no. 4, pp. 916–923, Aug 2018.

[5] K. Sreenath, N. Michael, and V. Kumar, "Trajectory generation and control of a quadrotor with a cable-suspended load - a differentially-flat hybrid system," in *2013 IEEE International Conference on Robotics and Automation*, May 2013, pp. 4888–4895.

[6] M. Guo, D. Gu, W. Zha, X. Zhu, and Y. Su, "Controlling a quadrotor carrying a cable-suspended load to pass through a window," *Journal of Intelligent & Robotic Systems*, 05 2019.

[7] A. Akhtar, C. Nielsen, and S. L. Waslander, "Path following using dynamic transverse feedback linearization for car-like robots," *IEEE Transactions on Robotics*, vol. 31, no. 2, pp. 269–279, April 2015.

[8] A. Akhtar and C. Nielsen, "Path following for a car-like robot using transverse feedback linearization and tangential dynamic extension," in *50th IEEE Conference on Decision and Control and European Control Conference, (CDC)-ECC*, Dec. 2011, pp. 7949 –7979.

[9] A. P. Aguiar, J. P. Hespanha, and P. V. Kokotović, "Performance limitations in reference tracking and path following for nonlinear systems," *Automatica*, vol. 44, no. 3, pp. 598–610, 2008.

[10] C. Nielsen, C. Fulford, and M. Maggiore, "Brief paper: Path following using transverse feedback linearization: Application to a maglev positioning system," *Automatica*, vol. 46, no. 3, pp. 585–590, 2010.

[11] D. Mellinger and V. Kumar, "Minimum snap trajectory generation and control for quadrotors," in *2011 IEEE International Conference on Robotics and Automation*, May 2011, pp. 2520–2525.

[12] A. Akhtar, S. Saleem, and S. L. Waslander, "Path following for a class of underactuated systems using global parameterization," *IEEE Access*, vol. 8, pp. 34 737–34 749, 2020.

[13] D. C. Gandolfo, L. R. Salinas, A. Brandão, and J. M. Toibero, "Stable path-following control for a quadrotor helicopter considering energy consumption," *IEEE Transactions on Control Systems Technology*, vol. 25, no. 4, pp. 1423–1430, July 2017.

[14] K. Sreenath, T. Lee, and V. Kumar, "Geometric control and differential flatness of a quadrotor uav with a cable-suspended load," in *52nd IEEE Conference on Decision and Control*, Dec 2013, pp. 2269–2274.

[15] A. Akhtar and S. Waslander, "Controller class for rigid body tracking on SO(3) (accepted)," *IEEE Transactions on Automatic Control*, 2021 (to appear).

[16] T. Lee, "Geometric control of quadrotor uavs transporting a cable-suspended rigid body," *IEEE Transactions on Control Systems Technology*, vol. 26, no. 1, pp. 255–264, Jan 2018.

[17] J. Zeng, P. Kotaru, and K. Sreenath, "Geometric control and differential flatness of a quadrotor uav with load suspended from a pulley," in *2019 American Control Conference (ACC)*, July 2019, pp. 2420–2427.

[18] P. Kotaru, G. Wu, and K. Sreenath, "Dynamics and control of a quadrotor with a payload suspended through an elastic cable," in *2017 American Control Conference (ACC)*, May 2017, pp. 3906–3913.

[19] T. Lee, K. Sreenath, and V. Kumar, "Geometric control of cooperating multiple quadrotor uavs with a suspended payload," in *52nd IEEE Conference on Decision and Control*, Dec 2013, pp. 5510–5515.

[20] J. Zeng and K. Sreenath, "Geometric control of a quadrotor with a load suspended from an offset," in *2019 American Control Conference (ACC)*, July 2019, pp. 3044–3050.

[21] M. Guo, D. Gu, and W. Zha, "Controlling a quadrotor carrying a cable-suspended load to pass through a window," *J Intell Robot Syst*, vol. 98, pp. 387–401, 2020.

[22] M. B. Mohiuddin and A. M. Abdallah, *Dynamic Modeling and Control of Quadrotor Slung-load System using PID and Nonlinear Backstepping Controller*. AIAA Scitech, 2021.

[23] P. O. Pereira and D. V. Dimarogonas, "Pose and position trajectory tracking for aerial transportation of a rod-like object," *Automatica*, vol. 109, p. 108547, 2019.

[24] T. Kusznir and J. Smoczek, "Quadrotor uav control for transportation of cable suspended payload," *Journal of KONES*, vol. 26, no. 2, pp. 77–84, 2019.

[25] A. Akhtar, S. L. Waslander, and C. Nielsen, "Path following for a quadrotor using dynamic extension and transverse feedback linearization," in *51st IEEE Conference on Decision and Control (CDC)*, Dec. 2012, pp. 3551 –3556.

[26] L. Qian and H. H. T. Liu, "Path-following control of a quadrotor uav with a cable-suspended payload under wind disturbances," *IEEE Transactions on Industrial Electronics*, vol. 67, no. 3, pp. 2021–2029, March 2020.

[27] P. Cruz and R. Fierro, "Cable-suspended load lifting by a quadrotor uav: hybrid model, trajectory generation, and control," *Autonomous Robots*, vol. 41, pp. 1629 – 1643, 04 2017.

[28] G. Wu and K. Sreenath, "Variation-based linearization of nonlinear systems evolving on $\mathsf{SO}(3)$ and $\mathbb{S}^2$," *IEEE Access*, vol. 3, pp. 1592–1604, 2015.

[29] G. Strang, *Linear Algebra and its applications*. 111 Fifth Avenue, New York, New York 10003: Academic Press, INC, 1976.

[30] C. Pugh, *Real Mathematical Analysis*. New York, U.S.A.: Springer, 2002.

[31] M. van Nieuwstadt, M. Rathinam, and R. M. Murray, "Differential flatness and absolute equivalence of nonlinear control systems," *SIAM J. Control and Optimization.*, vol. 36, no. 4, pp. 1225–1239, July 1998.

[32] Akhtar, Adeel, "Nonlinear and geometric controllers for rigid body vehicles," Ph.D. dissertation, University of Waterloo, 2018.